HecTO-R

One wing to deliver them all

NASA/DLR

Aeronautic Design Challenge 2020

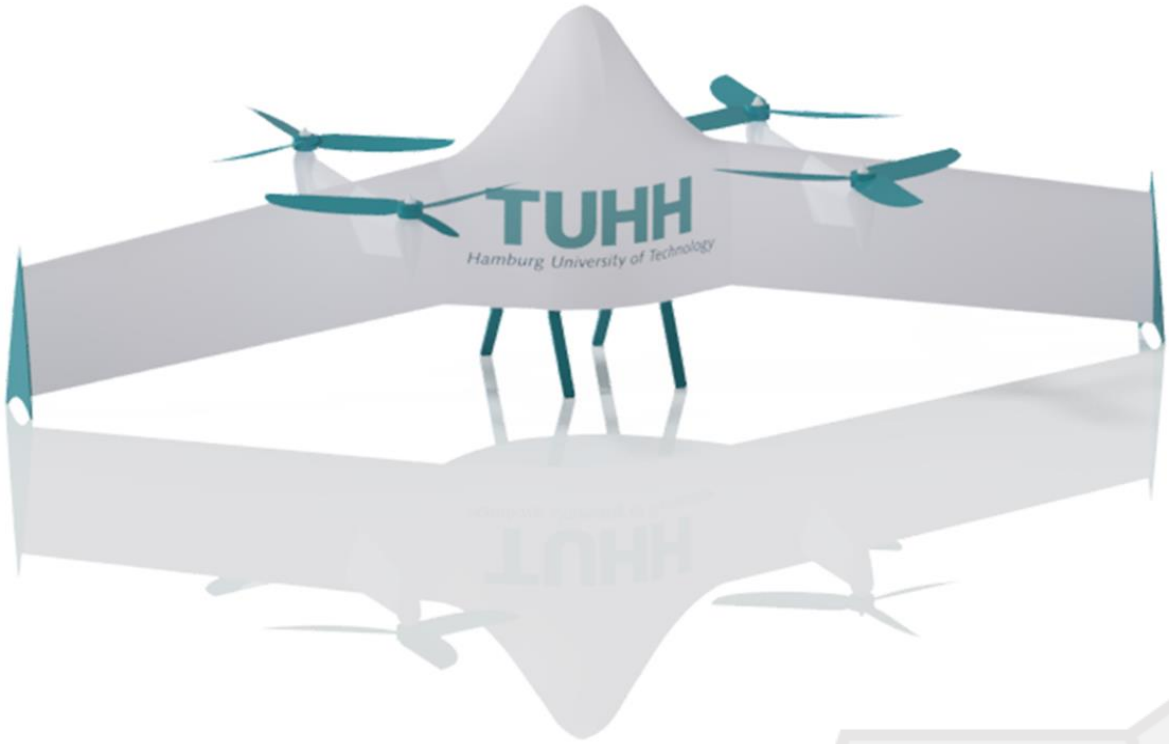

Team:
Anushan Thiripuvanam (Team Leader)
Flavio Geronimo, B.Sc.
Michael Szymanski
Niklas Schmidtke
Juan Felipe Ricardo Ramirez

Academic Support:
Prof. Dr.-Ing. Volker Gollnick
Jens Thöben, M.Sc.

TUHH
Technische Universität Hamburg

ILT
Institut für
Lufttransportsysteme

DLR

TUHH, Institut für Lufttransportsysteme, D-21079 Hamburg

Institut für Lufttransportsysteme
Prof. Dr.-Ing. Volker Gollnick
Blohmstr.20
D-21079 Hamburg

Datum und Zeichen Ihres Schreibens	Geschäftszeichen	Hamburg,
	Prof. Dr.-Ing. Volker Gollnick	13. Juli 2020

Bescheinigung und Freigabe des Beitrags zur DLR/NASA-Design- Challenge 2020

Hiermit wird bescheinigt, dass der Beitrag der Studierenden zum Studierendenwettbewerb DLR/NASA-Design-Challenge 2020 am Institut für Lufttransportsysteme geprüft und freigegeben wurde. Die Einreichung des Beitrags wird hiermit befürwortet.
Für weitere Rückfragen stehen Herr Jens Thöben, M.Sc. jens.thoeben@tuhh.de oder ich gerne zur Verfügung.

Mit freundlichen Grüßen

Volker Gollnick
Institutsleiter

Postanschrift
21071 Hamburg

Besucheranschrift
Blohmstraße 20
21079 Hamburg

Telefon
+49 (0) 40 428 78-4196

Fax
+49 (0) 40 428 78-2979
www.tu-harburg.de/ilt

E-Mail
volker.gollnick@tu-harburg.de

TUHH, Institut für Lufttransportsysteme, D-21079 Hamburg

Institut für Lufttransportsysteme
Prof. Dr.-Ing. Volker Gollnick
Blohmstr.20
D-21079 Hamburg

Datum und Zeichen Ihres Schreibens	Geschäftszeichen	Hamburg,
	Prof. Dr.-Ing. Volker Gollnick	13. Juli 2020

Bestätigung der eigenständigen Projektbearbeitung zur DLR/NASA-Design-Challenge 2020

Hiermit wird ausdrücklich bestätigt, dass

Herr Flavio Geronimo, TUHH
Herr Juan Felipe Ricardo Ramirez, TUHH
Herr Niklas Schmidtke, TUHH
Herr Michael Szymanski, TUHH
Herr Anushan Thiripuvanam, TUHH

den eingereichten Projektbericht sowie alle dahinter liegenden Arbeiten vollständig eigenständig und ausschließlich unter Zuhilfenahme der angegebenen Quellen erstellt haben. Für weitere Rückfragen stehen Herr Jens Thöben, M.Sc. jens.thoeben@tuhh.de oder ich gerne zur Verfügung.

Mit freundlichen Grüßen

Volker Gollnick
Institutsleiter

Postanschrift
21071 Hamburg

Telefon
+49 (0) 40 428 78-4196

E-Mail
volker.gollnick@tu-harburg.de

Besucheranschrift
Blohmstraße 20
21079 Hamburg

Fax
+49 (0) 40 428 78-2979
www.tu-harburg.de/ilt

Abstract

Within the scope of this year's Joint NASA/DLR Aeronautics Design Challenge the unmanned aerial vehicle (UAV) concept HecTO-R (ger.: Heckstarter Take-Off + Robot) aims to execute rapid and safe package deliveries in urban environments while being reliable, expandable and full electric with a green power supply. The project puts an emphasis on the current difficulties and requirements posing a challenge in the yet unexploited sector.

HecTO-R is a hybrid between a quadcopter and a blended-wing tailsitter, combining a vertical take-off and landing (VTOL) to a speedy cruise flight. The wings are optimized to provide stable and safe flight characteristics, minimizing possible accident risks. In order to not further deteriorate the air quality in cities, HecTO-R is powered by renewable energy stemming from Licerion High Energy (HE) lithium metal batteries, which have sufficient storage capacity for two missions. The avionics are selected in way that enables HecTO-R to communicate with the Unmanned Aircraft System Traffic Management (UTM) and to further avoid collisions with the use of an on-board detect-and-avoid system.

In order to reduce mass and costs, nearly all the components are manufactured out of carbon fiber reinforced polymers (CFRP). HecTO-R lands on foldable stilts located at the back of the fuselage. The light aluminium loading mechanism is integrated into the fuselage, which allows HecTO-R to place packages almost anywhere independently. In connection with HecTO-R's high speeds, it is suited to meet the increasing demand for express and essential deliveries. In the event of a crisis, HecTO-R is able to speedily carry out vital supply transports despite a lack of infrastructure. Combined with the low operating costs, this makes HecTO-R an operable concept for an unmanned flight system for transporting small packages.

The HecTO-R Team

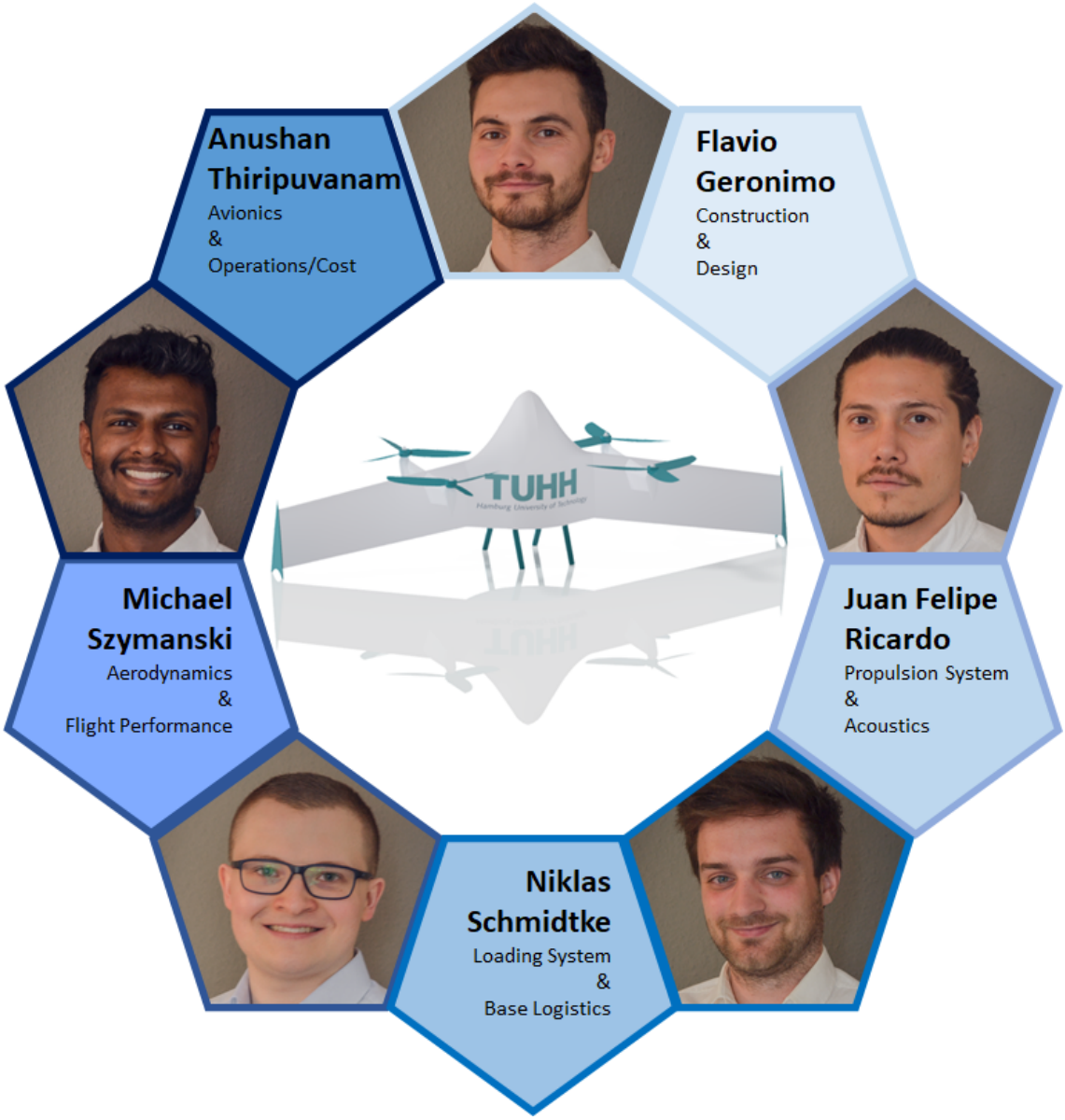

Contents

Nomenclature

Abbreviations

Abbreviation	Meaning
	A
A/D	Analog to digital
AC	Aerodynamic center
$ADS-B$	Automatic Dependent Surveillance - Broadcast
$AFDX$	Avionics Full-Duplex Switched Ethernet
AGL	Above ground level
AoA	Angle of attack
AoS	Angle of sideslip
ASL	Above sea level
$BLDC$	Brushless Direct Current electric motor
BVI	Blade vortex interaction
$BVLOS$	Beyond visual line Of sight
CAN	Controller Area Network
$CCDL$	Cross Channel Data Link
CG	Center of gravity
D/A	Digital to analog
$DGPS$	Differential Global Positioning System
DOC	Direct operating costs
$EASA$	European Union Aviation Safety Agency
ESC	Electronic speed controller
FAA	Federal Aviation Administration
$GALILEO$	(European) Global Navigation Satellite System
GCS	Ground control station
$GLONASS$	(Russian) Global Navigation Satellite System
$GNSS$	Global Navigation Satellite System
GPS	Global Positioning System
IC	Internal combustion
$ICAO$	International Civil Aviation Organization
IMA	Integrated Modular Avionic
IMU	Inertial Measurement Unit
IOC	Indirect operating costs
$LAANC$	Low Altitude Authorization and Notification Capability
$LiPo$	Lithium polymer
LoE	Law of effectiveness
MAC	Mean aerodynamic chord
$MEMS$	Micro-Electro-Mechanical Systems
NP	Neutral point of wing
$OASPL$	Overall sound pressure level
PID	Proportional–Integral–Derivative
QoS	Quality of service
$RAIM$	Receiver Autonomous Integrity Monitoring
RID	Remote Identification
$RTCA$	Radio Technical Commission for Aeronautic
SM	Static margin
T/O	Take-off
TAS	True air speed
$TLARD$	Top level aircraft requirement document
UAS	Unmanned Aerial System
UAV	Unmanned Aerial Vehicle
USS	Unmanned Aerial System Service Supplier
UTM	Unmanned Traffic Management
VLM	Vortex lattice method
VTO	Vertical take-off
$VTOL$	Vertical take-off and landing
$XFLR5$	Potential flow solver for subsonic airfoils and wings based on XFOIL

$XFOIL$	Analysis tool for subsonic airfoils

Greek Symbols

Symbol	Meaning
	G
α	Angle of attack
β	Angle between UAV and observer
η	Efficiency
γ	Angle of climb/descent
λ	Taper ratio
μ	Kinematic viscosity of air
$\phi_{1/4}$	Quarter chord sweep angle
ϕ_{Geo}	Geometric wing twist
ρ	Air density
θ	Pitch angle

Index

Symbol	Meaning
	I
0	Zero-lift
1/4	Quarter chord
Bat	Battery
BEW	Basic empty weight
CG	Center of gravity
eff	Efficiency
el	Electricity
Geo	Geometric
in	Input
M	Moment
MAC	Mean aerodynamic chord
max	Maximum
min	Minimum
$MTOW$	Maximum take-off weight
OEW	Operating empty weight
out	Output
P	Flight phases
p	Package
PL	Payload weight
$Prop$	Propeller
Req	To fulfill requirements
$Stall$	Stall configuration
tot	Total
$transfer$	Power transfer for motor and propeller
$Twist$	Due to geometric wing twist
v	Vehicle
W	Wing

Latin Symbols

Symbol	Meaning
	L
$(\frac{dC_M}{\phi_{Geo}})$	Moment coefficient due to geometric wing twist
$(\frac{dC_M}{dC_L})$	Static margin
$\bar{c}$	Mean aerodynamic chord length

$\frac{dL}{L_0}$	Lift ratio
AR	Aspect ratio
b	Wing span
C	Coefficient
c	Chord length
c	Cost
c_0	Speed of sound
D	Drag
$dSPL_{bv}$	Correction value to determine blade slap noise
e	Charging
g	Gravitational acceleration
i	Angle of incidence
L	Lift
M	Pitching moment
m	Mass
Ma	Mach number
n	Rotational speed
p	Power consumption of the electronic
r	Distance between propeller and observer
r	Lift to drag ratio
Re	Reynolds number
S	Wing reference surface
SPL_{mb}	Sound pressure level at a given ordinal number of the sound harmonic
T	Thrust
v	Aircraft speed (TAS)
W	Weight
X	Position along X-axis from reference
Y	Position along Y-axis from reference

1. Introduction

The mobility of people and goods in urban areas is increasingly reaching its limits. In order to maintain mobility despite constantly increasing movements and to simultaneously relieve road traffic, urban air mobility is considered a viable solution. As this is a global problem, this area of aviation is becoming more and more interesting for companies. New companies with promising concept technologies are continually entering the market to handle the large and growing demand for fast parcel delivery, making it currently the fastest growing area in aviation [Stü20]. Improved propulsion technologies and increasingly reliable and economical avionics enable the use of unmanned flight systems in public areas. The aim now is to develop a safe and secure, reliable, quiet and profitable delivery UAV within an ideally expandable program. By shifting the light parcel transport within urban regions into the airspace, UAV relaxes the road traffic by eliminating parcel transport and express delivery is made possible.

2. Requirements

The Top Level Aircraft Requirements consider the air vehicle's most important parameters and performance values. All necessary data is compiled in the TLARD (see in the appendices table 2). It is important that the air vehicle meets or outperforms all requirements set by the NASA/DLR commitee and/or regulatory frameworks such as CS-23 and CS-VLA, though not all points may apply due to the nature of the air vehicle and how most of its flight phases are performed. These regulations are still being or need to be developed at this point of time. The TLARD provides an overview of all crucial information regarding geometry, weight, mission planning, costs, time and functionalities in comparison to a direct competitor [Dre15].

3. Conceptual Design

3.1. UAV Design

For the conceptual design various different concepts were considered before deciding for a blended-wing quadcopter-tailsitter hybrid, which can be seen in the appendices figure 1 underneath and 17. This concept, HecTO-R, merges the advantages of a multicopter (i.e. VTOL, precise handling at slow speeds, hovering) and those of a blended-wing tailsitter (i.e. rapid VTOL, high cruise speeds, compact construction, improved aerodynamics).

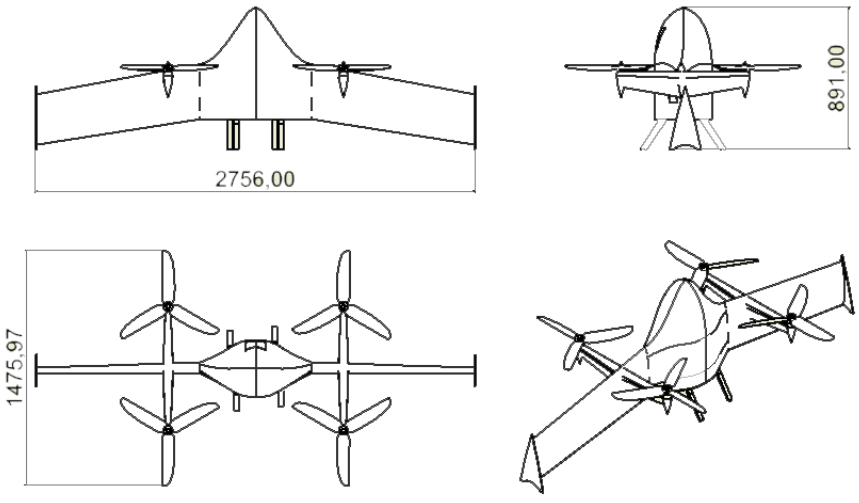

Figure 1: HecTO-R, three-side view

4. Technical Design

4.1. Aerodynamics

The aerodynamic evaluation and design of the flying wing represents one of the toughest challenges in the creation of the UAV. Due to the unconventional design choice the flying wing, which only provides a single lifting surface, requires unconventional trim and control capabilities. It is therefore of utmost importance to create an efficient and safe wing for varying conditions as required by the design challenge. It needs to provide sufficient lift and pitching moment stability during cruise and climb/approach phases as take-off T/O and landing happen fully vertical thanks to a quadcopter cross-arrangement of the propellers.
The first step in the creation of the wing is to set up all the necessary boundary conditions and requirements under which the flying wing needs to perform while also including first general assumptions, especially regarding masses $m_{max} = 26kg$ for the loaded and $m_{min} = 23,5kg$ for the unloaded air vehicle (see table 2 R3), which play a key role in the conception of the wing. The wing creation process therefore requires many iterations to fit the general project requirements as well as legal and structural limitations. Once all criteria are met one can further optimize and improve certain aspects of the flying wing. To meet all necessary requirements however, the first wing design needs to be estimated and calculated analytically with the use of empirical data whenever there is no other solution available. A simulation in XFLR5 using Vortex Lattice Method (VLM), which provides good and presentable first concept results is also made. This does not negate any further wind tunnel or CFD testing due to other existing types of interactions (mainly wing-body-propeller interaction) which cannot be solved analytically or using potential flow solvers like XFLR5. However, these methods require a lot more computational and monetary resources when solving numerically using a CFD solver or having access to wind tunnel testing facilities.

4.1.1. Wing Geometry & Layout

For the flying wing layout of the selected VTOL quadcopter/tailsitter hybrid UAV a single trapezoidal swept mid-wing configuration is chosen. This is done to move the aerodynamic center (AC) of the wing further aft. In total, the AC in the flying wing design is automatically the neutral point (NP) of the air vehicle since there are no other lifting surfaces besides the flying wing itself. This also excludes any types of wing-tail interactions (i.e. downwash effects) due of the lack of an empennage. Doing this also allows for the total center of gravity (CG) of the loaded and unloaded air vehicle to be moved further aft. This is necessary due to the loading compartment's and payload position's need of being within or, optimally, at static margin (SM) as well as needing to be as close to the platform as, ideally, the maximum payload height to minimize vertical loading/unloading distances. SM is discussed later in chapter 4.1.3. Hence the sweeping of the wing comes in handy since while the flying wing is on the ground it is in vertical configuration, the wing tips being much closer to the ground than the root where the fuselage is positioned. Once the wing and fuselage parameters are chosen wisely, this allows for the payload to be loaded from below the air vehicle and therefore from aft to nose instead of sideways (air vehicle nose pointing towards zenith and air vehicle aft pointing towards nadir when in vertical orientation), reducing the travel distance between platform and cargo by minimizing potentially wasted space. The loading/unloading mechanism is presented in chapter 4.5.1.
Accounting for these and many other geometric limitations sets first general boundary conditions for the air vehicle size. This helps with minimizing the necessary fuselage diameter and decreasing the occupied space by the air vehicle on the landing platform resulting in a tailor-fit air vehicle that checks all requirements.
Since the wing is constrained by those parameters, all other geometric sizes of the wing need to follow suit and be adjusted wherever possible to maximize efficiency, stability and functionality. Additionally, thanks to the use of spreadsheets it is possible to determine other crucial geometry figures, which could be monitored and checked whenever an adjustment to the wing geometry is made to further fit or fulfill specifications. The wing is adjusted for a chosen fixed wing span b, an AR between 5-9 to have a well balanced wing, a fixed root chord length c_{root} that best matches fuselage length and a small quarter chord sweep angle $\phi_{1/4} < 15°$ to minimize any potential drawbacks due to sweeping while at the same time improving directional and lateral stability features. The equations for the geometric calculation of the wing can be found in *Gudmundsson* [Gud16a] and geometric values are given in the appendices table 3.
Adding a canard design to the fuselage was taken into consideration before being discarded due to the additional actuators and mass. Further, it would also have shifted the NP and SM, potentially making the UAV unstable. Lastly, having an empennage as used in conventional air vehicle designs would not allow for quadcopter-like vertical T/O or landing and would hinder the loading mechanism.

4.1.2. Airfoil Selection

Selecting the correct airfoil required a lot of fine-tuning and the use of a different airfoil series beside the typical 4-series NACA airfoils. This decision is made to fit all necessary design and stability requirements the air vehicle has to fulfill for level flight meaning the air vehicle needs to be inherently stable at cruise flight. Generally speaking, airfoils with superior lift and stall qualities and a mainly positive zero lift moment coefficient $C_{M0} \geq 0$ at given subsonic Mach and Reynolds numbers are chosen. While cambered 4-series NACA profiles are very popular airfoils used in general aviation, they are not designed for flying wings because all cambered NACA 4-series airfoils provide negative C_{M0}.
To achieve the necessary characteristics, a profile with a negative, also called "reflexed", camber is necessary for flying wings in combination with small sweep angles. This could be achieved by flipping a NACA airfoil upside-down but it would overall decrease lift and stall capabilities. It would also be possible to only use a symmetric airfoil if the concept of geometric wing twisting is introduced. The issue with this approach is that it would either require increased wing sweeping combined with a wider wing span b and/or a lot of geometric wing twisting to induce the required zero-lift moment coefficient if the other values cannot be changed, which they mostly cannot. Therefore, the use of two airfoils at root and tip (aerodynamic twisting) is required.
To have a first performance evaluation of the combined MH-/NACA-airfoil, data for both airfoils at given Reynolds numbers is found in [Wet20], an online library for all types of airfoils based on 2D XFOIL simulations, and compared. To create first analytical values by assuming a bell-shaped lifting curve for trapezoidal wings, it is necessary to have all stall and zero lift information regarding lift, drag and pitching moment coefficients for each airfoil. It is then possible to establish first lift and drag coefficients for the selected tip and root airfoils by assuming a linear increase in lift from zero lift up until stall angle of attack AoA. Later, the calculated values of tip and root airfoils are combined by using the Law of Effectiveness LoE as applied in [Gud16b]. These combined and corrected values are the final reference coefficients of the wing (values given in reference to mean aerodynamic chord MAC). To linearize and correct the combined values for a swept and finite 3D wing, the approach referenced in [Gud16c] is used for estimating first lift and drag coefficients of the real wing. For the profile drag estimations of the non-lifting main components like the fuselage and engine pylons methods such as described in *Gollnick* [Gol19] are used to calculate the total profile drag of the air vehicle. The total profile drag coefficient is calculated as follows:

$$C_{D0} = C_{D0,W} + \Sigma C_{F,i} \cdot F_i \cdot Q_i \cdot (\frac{S_{Wetted,i}}{S}) \tag{1}$$

with $C_{D0,Wing}$ being the wing zero-lift drag as calculated using the Law of Effectiveness to combine both wing profiles, $C_{F,i}$ being the surface friction coefficient, F_i the form factor, Q_i the interference factor and $S_{Wetted,i}$ the wetted surface of each component. For the final wing design the MH-78 airfoil specifically used for flying wings designed by Dr. Martin Hepperle (see *Hepperle* [Hep18]) has proven to be the best choice for the root profile considering lift, drag, stall, pitching moment and stability aspects during aerodynamic analysis of the wing. Furthermore, the above mentioned concepts of aerodynamic and geometric wing twisting are added to further maximize safety, stalling behavior and stability during cruise. Therefore, for the tip airfoil a symmetrical airfoil is selected, specifically the NACA 0012 airfoil. The calculations and correct application and combination of both twisting methods are described in [Gud16d].
All final wing data regarding geometry and airfoil selection is given in table 3.

4.1.3. Longitudinal Static Stability

The final step in the conceptual wing design procedure is to validate longitudinal static stability for the air vehicle during cruise. Validating longitudinal static stability marks a very crucial milestone in the design process. It confirms that the air vehicle is capable of maintaining and returning to a statically stable longitudinal flight condition by itself. For this to be valid, two important requirements need to be met for an inherently stable flying wing and any other air vehicle: The total zero lift moment coefficient $C_{M0,tot}$ needs to be greater than 0:

$$C_{M0,tot} = C_{M0,W} + C_{M0,Twist} > 0 \tag{2}$$

The desired static margin SM needs to be smaller than 0. This requires CG to be in front of NP. SM is always given in proportion to MAC length:

$$(\frac{dC_M}{dC_L})_{desired} = SM = \frac{X_{CG} - X_{MAC}}{\bar{c}} < 0 \tag{3}$$

The closer CG is to NP, meaning that SM ≤ 0, the better the maneuverability of the air vehicle at the cost of stability. The further away CG is to NP, meaning that SM $\ll$ -0,1, the greater the stability of the air vehicle at the cost of maneuverability. Generally, a value between SM $\approx$ -0,05 and -0,1 is considered a good compromise between stability, maneuverability and payload position flexibility. For the design SM a value for $(\frac{dC_M}{dC_L})_{desired}$ at $-0,075$ is chosen. Should the actual SM change due to a change in total CG position the air vehicle can still be trimmed by using small amounts of differential thrust to counteract any changes in SM during flight while still maintaining good responsiveness. It is therefore important to keep the CG position of the payload at check for inherent pitch stability. By selecting the specific static margin it, retrospectively, also adjusts the required wing twist. The larger the static margin the greater the washout needs to be. This increases the moment due to linear wing twist $C_{M0,Twist}$ because a larger SM basically means a longer lever arm for the lift-induced moment.

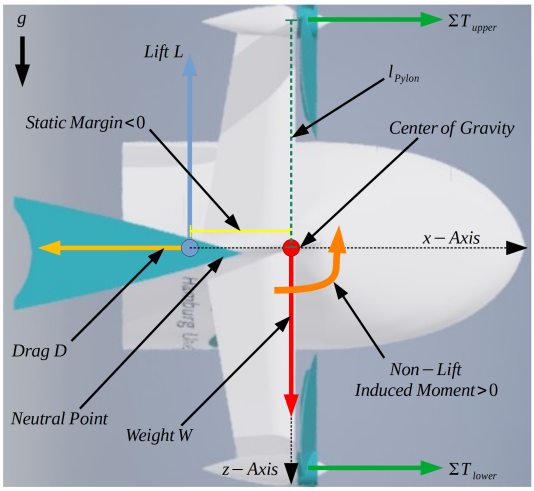

Figure 2: Longitudinal static stability of the flying wing with differential thrust

This gives us the following pitching moment coefficient equation which includes zero lift, twist, lift (see *Scholz* [Sch15a]) and differential thrust coefficient terms:

$$C_M = [C_{M0,W} + C_{M0,Twist} + (\frac{dC_M}{dC_L})_{desired} \cdot C_L] + [\frac{\Delta T \cdot l_{Pylon}}{0,5 \cdot \bar{c} \cdot \rho \cdot S \cdot v^2}] \tag{4}$$

with $\Delta T \times l_{Pylon}$ being the pitching moment due to a difference in thrust between the propellers above (upper) and below (lower) wing CG in z-Axis:

$$\Delta T \cdot l_{Pylon} = \Sigma T_{lower} \cdot l_{Pylon} - \Sigma T_{upper} \cdot l_{Pylon} = (\Sigma T_{lower} - \Sigma T_{upper}) \cdot l_{Pylon} \tag{5}$$

At the same time, this term expresses the capability of the propellers to have the air vehicle rotate around its CG at low speeds which allows for full horizontal and VTOL control of the air vehicle at below-stall speeds. This enables transitional maneuvers between vertical and horizontal flight and vice versa. These are very difficult to predict due to post-stall situations during these specific flight phases and requires further testing and simulations. The total pitching moment for such a maneuver can be expressed as follows:

$$\Sigma M = I_{yy} \cdot \ddot{\theta} = [0,5 \cdot \bar{c} \cdot \rho \cdot S \cdot v^2]([C_{M0,W} + C_{M0,Twist} + (\frac{dC_M}{dC_L})_{desired} \cdot C_L] + [\Delta T \cdot l_{Pylon}]) \tag{6}$$

However, for an inherently stable flying wing all acting moments must equate to 0. To avoid excessive use of differential thrust for trim its term needs to be minimized to 0 in equation 4.
The moment coefficient factor due to linear twist for a given air vehicle geometry $(\frac{dC_{M0}}{\phi_{Geo}})$ can be estimated using figure 3 with $\lambda \approx 1$ in this case. Multiplying it by the geometric twist angle ϕ_{Geo}, which is $-2°$ for the air vehicle, gives us the moment coefficient $C_{M0,Twist}$. The final coefficient $C_{M0,W}$ considers the combined zero lift moment coefficient of the wing itself as calculated using the LoE and accounts for wing sweeping (see *Scholz* [Sch15b]).

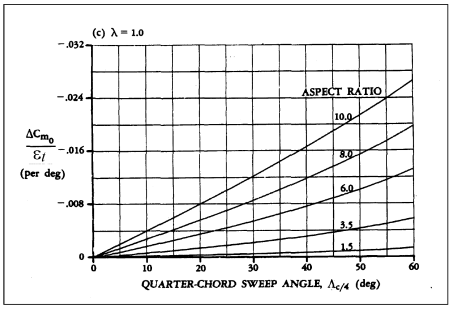

Figure 3: Influence of linear wing twist on pitching moment coefficient (see Scholz [Sch15b])

4.1.4. Aircraft Trim and Control

The only issue with this amount of design flexibility is that in the end decisions regarding air vehicle performance need to be made. It is therefore necessary to find a good twist angle for the given SM which could ensure static stability for all flight conditions and changes in CG. Setting the incidence angles for root and tip within reasonable range actively influences the cruise AoA and therefore $C_{L,Cruise}$ which for cruise is 0,33. This required the most iterations to get sophisticated and well balanced results as this would change many values, most notably v_{Cruise}. The lower the AoA, the lower $C_{L,Cruise}$ requiring a higher v_{Cruise} and vice versa. Since $C_{M0,W}$ and $C_{M0,Twist}$ are fixed values and the only trim device is the aforementioned differential

thrust, which is avoided during cruise, the only thing left to do for being able to fly at different altitudes and weight configurations is to adjust the air vehicle cruise speed v_{Cruise} to allow for the total lift coefficient $C_{L,Cruise}$ to be constant during all flight configurations so that lift L still equals W_{Max} or W_{min} as well as keep $C_{M,Cruise} = 0$. This means that the cruise speed v_{Cruise} becomes a function of air density at a given altitude above sea level ASL, a reasonably selected and fixed $C_{L,Cruise}$ and loaded/unloaded air vehicle weight W:

$$v_{Cruise}(\rho(ASL), W) = \sqrt{\frac{2 \cdot W}{\rho(ASL) \cdot S \cdot C_{L,Cruise}}} \tag{7}$$

It is therefore necessary to know the needed air vehicle cruise speeds for a given altitude, specifically for altitudes between 0m and 3000 m ASL and air vehicle weight as stated in the design requirements. Cruise speeds range between 35 m/s for the unloaded air vehicle at 0 m ASL and 43 m/s for the loaded air vehicle at 3000 m ASL (see table 2 R2.1). Having done that, it can be seen that the Reynolds and Mach numbers (at MAC as reference) did not change significantly, meaning that the airfoil profile information did not have to be further adjusted. This would have been required since airfoil coefficients are usually given for different Reynolds numbers. Here, the Reynolds number stays within a range of 800.000 to 1.000.000. Operating at Mach numbers above 0,3 would also require accounting for compressibility effects though the air vehicle flies at much lower speeds resulting in Mach number below 0,15. All calculated air vehicle speeds for different conditions exceed mission requirements. The biggest drawback in this approach is that it directly influences the needed propeller thrust and therefore power and energy needs when discussing flight performance in chapter 5 and battery sizing in chapter 4.6.3. In total, the air vehicle has two unconventional yet sufficient trim/control methods which cover a wide range of motion control and inherent stability features:

- Differential thrust $\Delta T \cdot l_{Pylon}$: used to trim and control the total air vehicle pitch, yaw and, to an extent, roll moments for either making transitional maneuvers (control) or maintaining longitudinal/directional/lateral static stability (trim).
- Variable Cruise Speed $v_{Cruise}(\rho(ASL), W)$: used to maintain lift-to-weight equilibrium L=W for given operating altitude ASL and weight (trim). This means a slight change in total thrust T is required to then overcome drag D at higher/lower speeds as, ideally, T = D during cruise. Performance aspects are discussed in chapter 5 and shown in figures 27 and 28.

Additionally, inherent directional and lateral stability are required if sideslip occurs due to asymmetric airflow over the wings and therefore asymmetric lift distribution on the wings. To guarantee directional/lateral stability, following methods are used to stabilize, trim and control sideslip-induced yawing/rolling motions and are qualitatively described:

- Wing sweeping: Wing sweeping towards aft creates a negative rolling moment coefficient slope through the origin adding to the dihedral effect for inherent roll stability.
- Winglets: Reduce induced drag and increase dihedral effect for inherent yaw stability similar to a wing fence or vertical stabilizer. Furthermore, they act as secondary landing gear.
- Ailerons: Control surfaces at the wing tips to control rolling motion. While the propeller arrangement follows a quadcopter x-shape design and allows for full pitch, yaw and rolling motions by controlling thrust and rotational moment of the propellers to either trim the air vehicle or do a controlled maneuver, ailerons are added as both a means of redundancy and to reduce dependency on the propellers.
- Differential thrust: As mentioned before, the specific propeller x-shape arrangement as both a trim or control device allows for pitch, yaw and roll motions.

Balancing out all of these methods creates a flying wing with inherent directional and lateral static stability with trim and maneuver control functionality around all air vehicle axes.

4.1.5. Evaluation and Validation using XFLR5

Having established and calculated all necessary flying wing data, the relevant information can be put into XFLR5 to validate the design using VLM for different flight conditions, specifically conditions at 0m and 3000 m ASL. While this program is clearly limited in its capabilities (see [Dep19]), it still delivers sufficient results for the airfoils, since it is using XFOIL for that and the flying wing, since the fuselage shall "blend" in with the wing. This tool also saves a good amount of time and calculation power when compared to any other CFD solver. It can therefore be assumed that for small air vehicle flying at low $Re \leq 10^6$ and $Ma < 0,3$ numbers, $XFLR5$ delivers reliable results for the flying wing. The results in figure 20 are calculated for cruise flight of a loaded and unloaded air vehicle at 0m and 3000m ASL each.

4.1.6. Conclusion Aerodynamics

Comparing the analytically calculated values to the simulation values in figure 20, matching results and longitudinal static stability can be validated. Also, the graphs for the different conditions and flight speeds overlap. This means that the combined analytical approach with given empirical data has proven successful in providing consistent and reliable aerodynamic information for these scenarios. However, for a more sophisticated design analysis it is necessary to determine directional and lateral static stability as well as the dynamic behavior of the flying wing and do further testing to determine stall behavior. Ideally, the straights in the lower left graph in the appendices figure 20 should need to go through the origin of the graph since the air vehicle's initial position is already set to cruise AoA. Therefore, this needs to be trimmed by using some differential thrust or by increasing the magnitude of the static margin very slightly. For a preliminary aerodynamic air vehicle design however, this shall suffice.

4.2. Materials

Strength, weight, and reliability are considered the most pivotal factors when selecting the materials used in the construction of an UAV. In order to both fulfill these requirements and guarantee an immediate entry into service through already available resources, the material selection falls on carbon fiber reinforced polymers (CFRP). CFRP components are a versatile essential in lightweight construction and are usually implemented in aerospace, shipbuilding, and the automotive industry due to their excellent strength-to-weight ratio. Therefore, it optimally withstands the various types and combinations of stresses an UAV encounters (tension, compression, torsion, bending, and shearing) whilst decreasing the weight in comparison to other materials. To absorb different loads, CFRP can be laid out in several layers with different fiber direction as shown in table 1 [RW92].

Stress	Fuselage	Wings	Fiber Orientation
Bending	Skins	Skins, spars, pylons	0° [1]
Shear	Skins, Frame	Spar webs	± 45° [1]
Torsion	Skins, Frame	Spar webs	± 45° [1]
Multiple stresses	Skins, Frame	Ribs, Pylons	0°/45°/90° Layers

Table 1: Stresses and resulting fiber orientation

In pursuance of a streamlined and economically efficient manufacturing process the blended wing UAV is constructed in CFRP parts merged with epoxy resin glue. The wing design features materials with both orthotropic and isotropic properties for improved strength. Thus, the CFRP main and rear spar are filled with polyurethane foam [Ada18]. On the wing, CFRP skins is glued onto two ribs holding the spars. Considering the complex shape of the fuselage, two half molds of conventional carbon roving are applied on the frame as can be seen in the appendices figure 18.

Since CFRP has low electrically conductive properties, it is susceptible to lightning strikes. Thus, a conductive mesh is interwoven in the surface of the CFRP skins. Of the eligible materials such as copper, bronze, or aluminium the latter is chosen due to its superior lightweight properties.

4.3. Fuselage

The fuselage has multiple design requirements giving it its shape. Firstly, it seamlessly blends with the wings to achieve the blended wing aerodynamics while carrying the frame with the spars. Secondly, it houses the batteries and avionic bays. These are located in dedicated spaces between the spars towards the wing profile and at the front of the fuselage. Thirdly, the payload loading mechanism is entirely accommodated. Initially, a rough elliptical bullet shape is designed to meet all the requirements. Upon accomplishment the fuselage shape is improved and streamlined further.

4.4. Landing Gear

The landing gear for HecTO-R is subdivided in a primary and a secondary landing gear. The former is composed of four foldable stilts, the latter is located at the back end of the winglets, keeping the UAV stable on the ground with enough clearance to not damage the wings. Since the UAV is able to hover, the landing impact on the stilts is minimal. Therefore, these are designed to hold HecTO-R's full weight and are manufactured out of aluminum, in order to rather slightly deform than instantly break in case of rough impact. The stilts are controlled by two rotational servo motors and are located at the bottom of the fuselage, leaving enough space between them for Roll-E to load the package into the loading mechanism.

Furthermore, the foldable mechanism reduces friction for take-off compared to fixed stilts. At all contact points with the ground a small rubber base ensures grip.

4.5. Operational Concept

HecTO-R's mission plan with the shortest and the longest flight duration is shown in the Appendices figure 30. The longest flight duration (bidirectional 23,28 min) is with an unloaded HecTO-R starting from 0 m ASL and the corresponding shortest flight (bidirectional 20,36 min) duration is with an loaded HecTO-R starting from 3000 m ASL. This results from lower cruise speeds at the unloaded stage due to the flight performances described in chapter 4.1.4 equation 7. In reality HecTO-R operates within the considered range of cruise speed and delivery duration. After each second bidirectional mission, HecTO-R's batteries are changed. This maintenance duration is estimated with 2 min, which leads to total flight duration of 42,72 - 48,56 min for two missions or 60 km. These properties clearly outperform the required flight duration of 80 min for two missions or 60 km.

4.5.1. Cargo

4.5.1.1. Loading

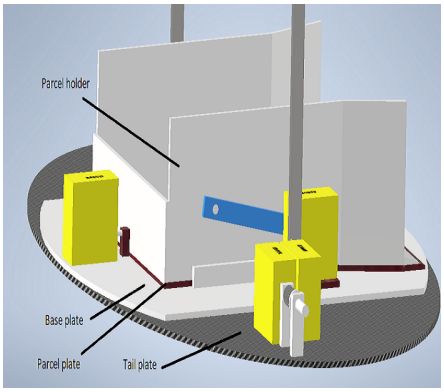

Figure 4: Loading mechanism, lateral view

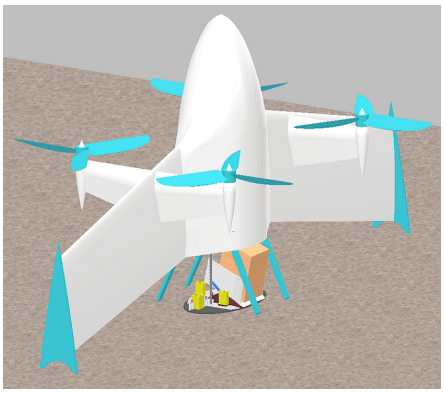

Figure 5: Mechanism while unloading

In order to minimise the needed landing precision, an electric tracked robotic vehicle (Roll-E), shown in figure 6, is used for cargo loading. Roll-E carries stops for picking up the parcel and two motors which move and fix the parcel. To pick up the parcel, Roll-E moves on his independently movable chains to the end of a conveyor belt, where the parcel is picked up fixed by a pin. With the help of cameras, used for orientation on the base, Roll-E then autonomously advances to the starting platform. While Roll-E is underway to bring the parcel to the UAV, it can communicate with HecTO-R via an ADS-B receiver. Meanwhile HecTO-R unlocks the base plate, which is locked to two sides of the fuselage by a wedge and consequently lowers down the base plate onto the tail plate. This is accomplished by a stepping motor, which moves the base plate vertically via cross-racks with two gear/rack connections. Once the base plate has reached the tail plate, the tail plate is locked to it by two pins, again both actuated by a linear servo motor each. Thereafter, two further pins, which lock the tail plate to the fuselage, are unlocked and the tail plate with the locked base plate on it are lowered down to the bottom of the launch platform. With help of light barrier systems installed on both, Roll-E positions itself perpendicular to HecTO-R, so that the parcel can be transferred into the pick-up area on HecTO-R's tail plate as shown in C.3 figure 21.

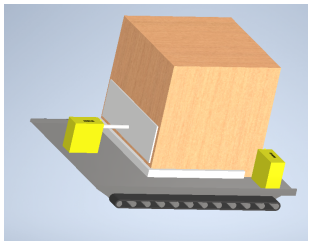

Figure 6: Loading robot, Roll-E

In order to prevent jamming during transfer, the package area on HecTO-R is widened at the front. To reduce friction during the parcel transfer, plastic spheres are installed in the package plate. Once the package is dispatched, Roll-E returns to the base. Meanwhile the base plate is raised until the rear plate is level with the outer fuselage skin of HecTO-R. Thereafter the tail plate is locked to the fuselage by the two pins again. Then the other two pins, are unlocked. The base plate moves upwards, driven by the stepper motor, until the parcel docks against the stop in the fuselage and the pins of the tailplate lock into the wedges in the fuselage, relieving the stepper motor. The loading mechanism in flight operation is shown in C.3 figure 22. HecTO-R is now ready for take-off.

4.5.1.2. Unloading

Upon arrival on the landing platform, floor plate with the parcel is lowered onto the tail plate, releasing the locking mechanism of the parcel. When the base plate reaches the tail plate, it is coupled again via the two pins and both plates move down onto the platform ground.
Now the parcel holder is tilted via two servo motors, which are mounted to a parcel plate underneath when widening the platform as shown in figure 5. To ensure that the parcel is no longer on any loading mechanism components, a linear servo motor is used to move both the parcel plate and the tilted parcel holder horizontally. Once the parcel is successfully unloaded, the loading mechanism lifts up, the tail plate locks to the fuselage again and HecTO-R is ready for take-off. The autonomous unloading process enables HecTO-R to deliver parcels without any further aids wherever there is sufficient free space to land.

4.5.1.3. Base

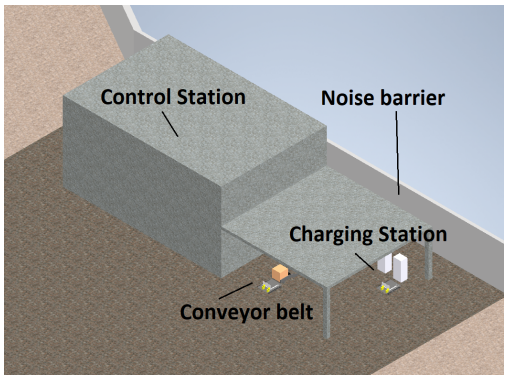

Figure 7: Base

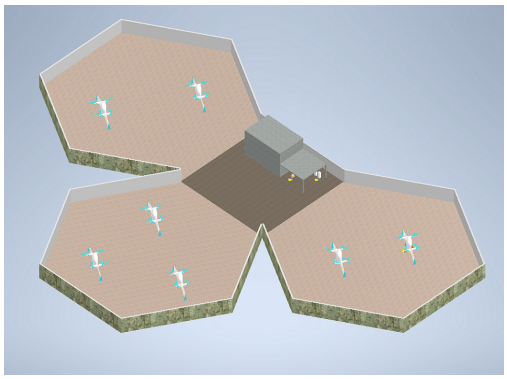

Figure 8: Base and launch platforms

The base is positioned centrally with several launch platforms laid out around it. The conveyor, the control station, the loading station and the storage area for the Roll-E are all located on the base and partly in the ground control station (GCS). To achieve a noise during of up to 20 dB take-off, the base and the launch platforms are surrounded by an approximately 3m high noise barrier [Umw20]. It mainly absorbs the usually regarded as disturbing high frequencies, reducing the most bothersome tones [Gol20]. In addition, it prevents people from entering and Roll-E's from driving off the platform in case of a wrongly calculated maneuver. Further noise reduction measures are described in chapter 4.7.

To start a mission every two minutes seven HecTO-Rs and three Roll-Es are required, of which one HecTo-R and one Roll-E are kept as back-up. By hypothetically modifying the parcel area on the Roll-E, it would be possible to pick up several parcels at the same time, thus achieving a reduction in handling time. HecTO-R's battery life is designed to complete two missions whereafter its batteries get replaced by an employee. Since the UAVs take off and land vertically, two can use the launch platform simultaneously, so that only three launch platforms are needed for the mission plan. These are expandable so that a higher clock rate would be achievable.

4.6. Propulsion System

The propulsion system is composed of battery packs, propellers, Electronic Speed Controllers (ESC) and motors. The system that is implemented in HecTO-R is composed of four 3-blade propeller, motor and ESC sets, all being powered by a central battery, described in chapter 4.6.5. The ESC receives the Pulse Width Modulation (PWM) control signals from the autopilot system mentioned in chapter 4.8.5 to control the movement of the UAV. Propeller sizing and performance calculations are found in chapter 5.2.2 and the needed power, thrust and velocity are referenced in the appendices figure 28.

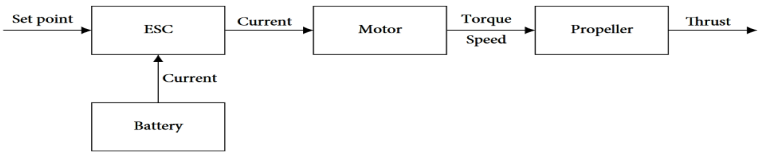

Figure 9: Propulsion system chain diagram

4.6.1. Motor

Considering the necessities of the system regarding hovering, the system has to be able to take-off without any problems and withstand the surrounding conditions. Therefore it is necessary to implement motors that are able to supply the maximum required power. The implementation of high pole Multi-Rotor BLDC motors [al19c] is the technology that covers the security, thrust and reliability necessities of the system and shows the following characteristics:

- high torque-to-weight ratio
- long lifespan
- near elimination of electromagnetic interference
- lower mass moment of inertia & higher rotational inertia
- low but constant speeds
- lightweight

The disadvantages are the higher costs for the magnet material and the controller, although the financial difference is likely to become smaller in the future. Brushless motors become more widespread in model flying and with it the associated mass production, as well as the further development of electronic components.
Because of the multicopter's propulsive control scheme, the motors need to be oversized (beyond of what is necessary for hover) to maneuver at constant altitude. Rotor inertia also impose control delays: The bigger the rotor, the longer the delay. To reduce the delay, the implementation of a Phase Delay Compensation (PDC) is foreseen and will be explained in the next chapter 4.6.2. Using the modelling program eCalc [Mül20] approximated data with the implemented system in HecTOR is obtained. The performance results are shown in table 5. According to the results and taking into account that these results have a 15% inaccuracy, the approximation of the motor efficiency is settled to be $eta_{transfer} = 81\%$.
The required motor provides the specifications described in chapter C.4.1 table 4 [Dir20b].

4.6.2. Electronic Speed Controller (ESC)

The ESC's function within the propulsion system is to regulate the speed of the motor by adjusting the timing of the pulse current delivered to several motor windings. Therefore it has to be designed according to the current requirements of the motor.
The implemented technology on the system is optimized regarding the aforementioned characteristics and has incorporated technologies as CANbus multiplex network serial-bus controls. Furthermore, by using telemetry and advanced motor control algorithms an optimal flight performance is assured. The implementation of Phase delay compensation (PDC) leads to delay reductions in the motor response, which is taken into account to withstand the different flight conditions. The proposed PDC method is realized by a digital logic circuit and a microprocessor, which is based on a Fourier-series-based PDC to improve the output torque and power efficiency at high velocities[[Kon18]]. The ESC is also tuned for peak performance and plug-and-play compatibility up to 14S HV (63.0V Max) input power for the thrust generation and peak efficiency output. In addition an appropriate resistance with regard to high temperatures (200°C), different weather conditions (rain and snow), dust, debris and vibration is achieved. Moreover the current and voltage monitoring leads to a reliable operation and the regenerative braking effects an instantaneous response to the flight controller commands[Dir20a].
The ESC's specifications are shown in the appendices table 6.

4.6.3. Battery

The energy supply is provided by a new technology: High Energy (HE) lithium-metal rechargeable batteries. The mentioned technology protects the lithium metal anode with three levels of protection as shown in chapter C.4.3 figure 23. With the protected lithium anode technology the anode is physically protected by a thin, chemical stable, and ionically conductive ceramic polymer barrier. At the cell-level, electrolyte additives chemically stabilize the anode surface to enhance cycle life and increase energy. The cells do have a liquid electrolyte whose amount is negligible compared to regular Li-ion cells. These batteries are ultra-high-energy (500Wh/kg), have long life-cycles (up to 1000 cycles depending on usage profile) and present possible charging times of 15 min with a charging efficiency of $e_{eff} = 99,7\%$ [gre20] [Pow20b][Bal20].The security of the device and the surroundings is granted while operating under normal conditions. More detailed information of the technology is given in table 7. The presented technology is to be commercialized in mid-2021 for UAV markets [Cor20] [Bal20].

4.6.4. Energy Consumption

The implementation of maximum efficiency components leads to a reduction of HecTO-R's energy consumption. For this reason, components such as motors, electric speed controllers (ESCs) and propellers must be chosen so that their interaction operate at maximum efficiency. Since the selected propulsion system is already optimized to generate the maximum amount of thrust while maintaining energy efficiency, the system has the following consumption characteristics divided into the different phases of operation:
The maximum power requirement amounts to approximately 20 kW, which needs to be supplied by the battery.
The required power multiplied with the corresponding times of each phase amounts to the total required battery energy. For the complete mission of two deliveries this equals to approximately 923 Wh for the propulsion system and 45 Wh for the electronics system. The battery mass is then estimated as follows:

$$m_{Battery} = \frac{\int P dt}{500 \frac{Wh}{kg}} \leq 3kg \tag{8}$$

4.6.5. Battery Configuration

Given that the maximum required power output taking place at the vertical take-off (VTO) and the transition from VTO to cruise flight (20 kW for less than 10 s), the battery needs to be configured to ensure the maximum required input power for the 4 motors.
With a battery module configured in 14 cells in series and three of the 14s-modules in parallel resulting in a 14s3p battery system the power and energy necessities for the propulsion system as well as redundancy are ensured. Covering the complete mission under consideration of the maximal discharge rate of the battery (80%) leads to 10% - 20% extra power for eventual inconveniences that may appear in-flight. The battery module is stored in the main bay shown in figure 18 in the appendices.
The implementation of an additional High Voltage Lithium-Polymer (LiPo) battery (6s1p) with high discharge rates ensures a glide autonomy if the main energy system fails, which leads to a higher safety. Further emergency systems are described in chapter 4.9.
The utilized battery technology shows a big energy density which enables a higher endurance and results in longer range. However, its disadvantage is that it needs very high continuous current draw during transition. It can be expected that the implemented technology will present improvements over time in terms of maximum power density and discharge rate. The battery needs to ensure both maximum power and energy draw but the proposed layout of a 14s3p battery system right now is too heavy for operation (6,6 kg). Here, further improvements need to be made in regards to battery power density, maximum discharge rate, motor velocity constant or overall air vehicle weight to reduce battery power needs and, subsequently, battery weight. If the battery is sized according to energy requirements in equation 8 it would only require a single 14s-battery module. However, the discharge rate for this type of configuration would be at least 18 C. Since most LiPo batteries have even higher discharge rates at 25-50 C it is expected that the proposed battery may improve over time.

4.7. Acoustics

Aircraft noise is typically dominated by propulsion. In small delivery drones, electric propulsion can eliminate the noise source associated with internal combustion (IC) engines. In most propeller-driven configurations rotor noise dominates other sources of noise (e.g. the engine and airframe). The following rotor-design parameters affect the noise emission: rotor material, tip speed, thickness, blade count, sweep, tip shape and blade twist. With the implemented propeller (28 in x 20 in) system the approximated maximum reachable tip speed is to be settled to Ma = 0,6 which is in the subsonic regime but will only be achieved at maximum throttle. Therefore the thickness noise is less relevant compared to other noise sources.
The dominant noise sources are the Blade Vortex Interaction (BVI), Broadband Noise and steady loading noises. By implementing larger propellers with lower rotational speed and therefore lower tip speed a reduction of such emitted noises can be achieved. Consequently, the unweighted radiated noise levels are reduced to smaller propellers, which generally require higher RPM while producing the same thrust. Shifting the noise towards lower frequencies results in a significant reduction in the A-weighted sound pressure levels and leads to the important reduction of the blade rate tones due to the lower needed velocities to generate the required thrust [al19d].
By implementing a narrow-serrated-porous (NSP) trailing edge a broadband noise reduction may be achieved. This can lead to a reduction of the Overall Sound Pressure Level (OASPL) by up to 14,2 dB (at frequencies from 250 Hz to 1000 Hz) as is presented in [al19c] and [al19a].
As described in chapter 4.5.1.3 the installed noise protection walls at the ground platform effect a noise reduction up to 20 dB.

Regarding the supplied customers, which are described in chapter 6.3, it is also necessary to mention the existing aircraft noise limits. Delivering to a specific landing platform with installed noise protection walls is viable without any problems even at night. Deliveries for emergency purposes (e.g. vital organs to hospitals) is also operable due to exceptional rules [Gie05]. Transportation to individual customers is conceivable as well due to an average noise limitation amounting to 65 dB published by the FAA [FAA18] which is in compliance with HecTO-R's operations.
As an approximation to determine the emitted noise, the blade slap noise has been calculated since it can be categorized in the noise source of blade vortex interaction and these emitted noises are predominant while flying. Considering the equation

$$SPL_{mb} = 20 * log(\frac{\Delta L}{L}\cos(\beta)) + 20 * log(\frac{T * n}{\rho * c_o^3 * r}) + \Delta SPL_{bv} + 190,2 \tag{9}$$

with the following parameters for take-off $\frac{\Delta L}{L} = 0{,}15$ for a conventional blade and $\frac{\Delta L}{L} = 0{,}07$ with blades with blade tip air injection , $\beta = 0, T = 430N, n = 116,61/s$ and $r = 10m$. Taking into account the aforementioned measures to noise reduction (protection walls, NSP trailing edge blade with tip air injection) an emitted noise value of $SPL_{mb} = 51dB$ is obtained. At a longer distance, with $r = 60m$, the emitted noise approximates to $SPL_{mb} = 35dB$. Due to the cruise altitude and reductions of both thrust and power, a lower noise emission compared to the take-off, is expected.

4.8. Avionics

Due to the complexity and vast amount of information related to HecTO-R's controlling a reliable, secure, light weight and fast data transfer is required. Critical systems like the flight control need to react as fast as possible considering HecTO-R's high cruise speed (see TLARD R 2.1) and possible evasive actions triggered by bird occurrence or emergencies. Furthermore these critical systems need to have a failure probability per flight hour of $< 10^{-9}$ [God20b]. The requirements are met through hardware redundancy and software diversity. The software itself is developed to meet the requirements for DO-178 Level A certification by Radio Technical Commission for Aeronautic (RTCA).
By using Integrated Modular Avionic (IMA) for the design of avionic compartments the computing efficiency and the costs can be reduced. To obtain higher redundancy the avionic compartments are installed by the principle of segregation in three different avionic bays regarding the data and resources they need. The main avionic bay is in the top; the left and right avionic bays are in the blended fuselage parts on both sides as shown in the appendices figure 18. To increase the fault tolerance of the software, static redundancy in form of triple modular redundancy is used. Three independent algorithms are used to calculate the required values. Afterwards the voter will choose two of three or the most appropriate output which will lead to fault masking and therefore to a higher fault tolerance.
The communication data transfer is implemented regarding the size and priority of data: High prioritized data or large data files such as the rotor control or the camera detect-and-avoid system (described in chapter 4.8.3) are shared with Aeronautical Radio Incorporated (ARINC) 664 Part 7 Standard, Avionics Full-Duplex Switched Ethernet (AFDX) which is based on the Ethernet IEEE 802.3 network standard. The information is transferred by the Quality of Services (QoS) feature, where prioritized data is transmitted first. The data is transferred through fiber optic cables, which leads to transfer rates up to 10 GB/s [God20a]. The use of fiber optic cables generates higher reliability, electromagnetic interference immunity, high bandwidth. These properties are advantageous due to the high broadband data transfer triggered by several avionic systems like the camera, 3D-mapping or continuous communication systems, which are described in the following chapters.
Moreover a reduction of unnecessary hardware redundancy is achieved by using Cross Channel Data Link (CCDL) [Bry12]. Through the use of CCDL specific data such as the angle of attack (AoA), obtained by the AoA sensors, is shared to different avionic compartments leading to a more efficient data transfer and less hardware mass.
In case of a limited functionality of the AFDX network, critical systems like the engine controls for the rotors have an own digital data link to the flight computers.
Lower prioritized data or smaller data files are transmitted through ARINC 825 Standard, Controller Area Network (CAN). The performance of CAN (data transfer rate of 83,33 KB/s - 1 MB/s) may be lower than the one of AFDX, but the operating environment, such as the communication of the ADS-B system (described in chapter 4.8.2) and the other sensors as the AoA sensors or digital barometer, do not require a high performance communication. In addition the costs of CAN based networks are lower than AFDX networks. Other possible standards like ARINC 429 or 629 are omitted due to a lower performance than ARINC 825 or higher costs than ARINC 664 Part 7 [Kop17][God20b].
By using a combination of ARINC 664 Part 7 and ARINC 825 a good equilibrium of cost reduction and high performance is obtained [Kop17].

Mechanism to reduce the danger of possible cyber attacks which could affect the functionality of the avionic networks are described in chapter 4.8.4.

4.8.1. Navigation Systems

Since urban area is usually a technically high developed region it also involves difficult requirements for the avionics of a UAV. Its automated landing process, as one of the highest safety-critical states, requires high precision vertical and horizontal positioning.
The relevant and available navigation systems are evaluated by considering the temporary stability divided into 4 criteria [TSt+08]:

- The general stability (behavior of the unprocessed sensor error over the time)
- Position-specific stability (temporary behavior of the effect of the sensor error over the positioning)
- Short-term stability
- Long-term stability

Global navigation satellite systems (GNSS) are generally, position-specifically and long-term stable albeit less short-term stable. The problem is reasoned by its sensitivity for electromagnetic interferences and other disturbances like ionospheric propagation and multipath propagation caused by a crowded, urban region. Therefore a combined solution, called sensor-fusion, is required, leading to a combination of GNSS and an inertial measurement unit (IMU).

An IMU is generally short-term and long-term stable. Using the IMU for positioning purpose leads to a long-term instability because of error propagation due to double integration and angular errors. Therefore it can be seen that a sensor-fusion of GNSS and IMU leads to an approximately overall stability [TSt+08].

The aforementioned interferences at GNSS signals still need to be considered. One possibility is the additional usage of pseudolites. Pseudolites are ground based signal stations whose position is exactly known. Simulating real additional navigation satellites results in a higher availability and precision for positioning. On the basis of the near-far problem (described in figure 10) the usage of pseudolite signals is only appropriate in the intermediate range. In the close and far range the GNSS signals and those of the pseudolites would overlap each other. What others see as a problem can be used here as an advantage: by choosing the right position for the starting and landing platforms, the intermediate range won't be passed due to the maximum mission radius of 15km. Therefore already existing pseudolites can be used. To still minimize the probability of overlapping signals a dynamic power control of the used transmitters or pulsed signals with different coding to those of the GNSS signals is used. Furthermore pseudolites are able to send signals of the differential global positioning system (DGPS). Using DGPS the accuracy of GNSS positioning is increased by transmitting correctional data with the aid of ground based reference stations. To ensure a minimum of electromagnetic interferences between the avionic parts and signals and to reach a maximum signal strength, the antenna needed are mounted outside of HecTO-R.

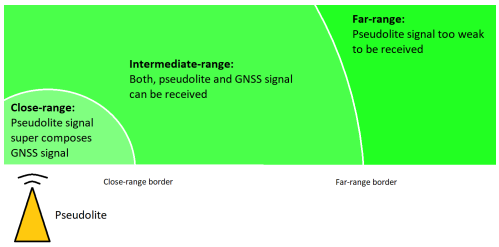

Figure 10: Near-Far problem

In order to reduce another source of error at GNSS positioning receiver autonomous integrity monitoring (RAIM) is used. With the help of RAIM erroneous navigation satellites can be excluded to maintain a correct and precise positioning. The high required number of navigation satellite signals can be ensured due to the launch of the European GNSS GALILEO. Combining the GNSS signals of the American global positioning system (GPS), the European GALILEO and the Russian global navigation satellite system (GLONASS) leads not only to the readily use of RAIM, it also increases the precision of GNSS positioning. Beside of these advantages RAIM can also be used against GNSS/GPS spoofing attacks, which is explained in chapter 4.8.4.

Even though high precision height measurements via the combined usage of the systems mentioned above is possible, additional redundant systems are recommended to have fail-operate features (e.g. occurring cyber attacks). Therefore several on-board measuring instruments, such as digital pressure sensors are used. Other used sensors are listed in the Top Level Aircraft Document (TLARD) under R7 in figure 2.

With the aid of all the systems described above a redundant and high precision navigation system can be provided which obtains a precision range of millimeters to centimeters. This also gives a great advantage in the strategic management of operations, where UAS with higher navigational performance can fly within smaller operation volumes which lead to a better integration of the UAS's operation into the traffic (management). More information in terms of operation volumes is given in chapter 4.8.3.

4.8.2. Identification System

On the basis of the increasing density in lower altitude aviation, a similar identification system to the already existing systems in manned aviation is necessary. The needed identification system enables the launch of an unmanned traffic management (UTM) system and has already been proposed by the federal aviation administration (FAA). According to FAA's latest publication in terms of the UTM [al20], the identification of the unmanned aerial vehicles (UAV) is to be performed by remote identification (RID).
The chosen standard RID is performed by network publishing: every HecTO-R is communicating online with its operator. The operator constitutes the management of the operation wherefore every HecTO-R needs internet access via mobile radio. The UAV sends a RID Message which includes a unique identification number (UAS ID), the location of the UAS and a time mark to its operator. The operator transmits the RID Message to a FAA qualified RID unmanned aerial system service supplier (USS) which makes the information publicly accessible through a distributed database. Furthermore the USS shares the information within a USS network which contains also a public safety USS where authorized public safety constitutions can obtain additional information like the operator's name and contact information. The structure of the UTM and its constitutions mentioned above is described in chapter C.5.1 figure 24 [al20].
Network publishing facilitates an identification system regardless of range, transmitting only chosen data. Nevertheless the usage of internet connection makes security measures essential, which are described in chapter 4.8.4.

As a result of legal situation and detect and avoid purposes (described in chapter 4.8.3) the usage of Automatic Dependent Surveillance - Broadcast (ADS-B) is necessary. The air vehicle gets (local) information like its flight route, velocity, cruise height etc. from their operator, satellites, altimeter etc. and broadcasts these information, similar to Mode-S Transponder, at 1090 MHz to the ground based flight control (called ADS-B out). The processed data are broadcasted from the ground station to all air vehicle which receives them (called ADS-B in) and therefore have information about air vehicle in near range which increases the situational awareness. Therefore the identification system via ADS-B is not only redundant in parallel to RID, it is also used to detect and avoid air vehicle in near range.
In some countries it is also necessary to carry an identification plate on HecTO-R. These aluminum plates include operator's information such as name, contact details and serial number.

4.8.3. Detect-and-avoid Systems

The aforementioned ADS-B Transponder in chapter 4.8.2 delivers information about nearby air vehicle which is used to avoid and inform nearby air vehicle.
Furthermore as figure 24 shows, the UTM network already delivers information about air vehicle in near range and even gives information about the detected come up of birds via the USS's Supplemental Data Service Provider and stakeholders. Although, the bird come up detection may not be reliable enough, which leads to a requirement of a further on-board detection system.
The UTM network analyses the flight trajectories via 4D separation: the trajectories are calculated by the mission plans delivered by the operators. The geographical and temporal data are used to create virtual volume segments wherein the individual air vehicle operates. If the UTM recognizes any virtual collisions it professes a temporal or spatial deconfliction to the operator and the UAS: either the UAS is controlled so that it reaches the point of eventual collision at a different time to the other air vehicle or it avoids the other air vehicle by changing its trajectory. This technology is described in chapter C.5.2 figure 25 and is later used in an independent detect-and-avoid system of HecTO-R.

Overall the featured detect-and-avoid systems work independently and offer additional information to increase situational awareness and flight safety.
The concepts for the UTM network also already include vehicle-to-vehicle ($V2V$ communication which works via dedicated short-range radio communication (DSRC) transponder and have a range of approximately 300m. The combined available systems lead to a great situational awareness between UAVs with the disadvantage that other UAV's must use the same systems and have to carry related devices. Also the mentioned systems don't include real time anti-bird strike systems which is an important issue at the operating height of 400ft AGL.

Therefore HecTO-R's detect-and-avoid system includes a 360 ° camera, which is combined with a high range RADAR to compare the sensor data and to obtain a more reliable detection. Existing algorithms for the camera can detect objects even in rain. In addition HecTO-R uses a lightweight and low-power camera system which lowers the overall energy consumption. There already are providers for those kind of cameras specifically developed for drones such as Casia by Iris Automation or Owl by RaptorPhotonics. Some of these cameras work with in-house software to detect other flying objects within a range of up to 500 m. Independent to the chosen provider for camera systems, an independent detect-and-avoid system via camera is described in chapter C.5.2 figure 26. The camera detects the object and calculates the displacement vectors via stain feature analysis and creates therefore a trajectory for the moving object. To obtain a better reliability of the trajectory, the stains leading to very different displacement vectors are excluded. This procedure is already described in [GKa90] which is more reliable and effective nowadays due to more powerful processors. The obtained trajectory, which is updated in real time, is used by an algorithm to detect an eventual collision and if necessary initiate evasive actions by HecTO-R. A conceptual and rough source code for these types of algorithms is shown in chapter C.5.2 listing 1. The UTM network also offers 4D-trajectories of the missions of each UAV (shown in figure 25), which are used to de-escalate any potential trajectory conflicts between UAVs.
For appropriate reaction to emergency and trajectory conflicts with security organs and their respective air vehicle, helicopters or drones, the information delivered by the FAA and the USS is used to avoid their trajectory. In exceptional cases emergency landings with the help of 3D mapping algorithms, described amongst other systems in chapter 4.9, can be executed.

Besides the aforementioned avoidance systems the air collision lighting, which is mandatory for dawn and night flights, can also be used to avoid bird strikes. Therefore statistical analysis of bird strikes are considered to give evidence about the visibility of certain bird species.
In general it can be noticed that birds mostly do detect air vehicle before a bird strike, however do not have enough time to avoid them. According to the experiment results in [Bla+12] the examined birds (e.g. Canadian gooses) react faster to alternating, pulsing lights at approximately 2 Hz. The more intense the lighting the faster the reaction of the birds. These results can also be transferred to the colors of an air vehicle: the lighter the color the better the detection by birds [Fer+11].
These information are used to install HecTO-R's bright, pulsing air collision lighting, which is activated in dependence of bird come up data by the UTM network & the visual detect-and-avoid system. In addition the UAV's detectability by birds is increased by choosing a light color scheme.

4.8.4. Security Systems

Due to progressing technologies like wireless data transfers and the increasing size of data files which have to be transmitted in less time, networks similar to those of UAVs are an interesting target group for potential hackers. Therefore every UAV need to implement appropriate security measures in order to resist those cyber attacks. Nevertheless it is important to mention that a 100% security against cyber attacks cannot be obtained. It is only possible to increase the difficulty for an attacker to hack the systems. Firstly, the most frequent cyber attacks are considered, as follows [Hic18]:

- Spoofing: Modified receiving signals or generated e.g. GPS signals to take control of the UAV
- Jamming: Jamming or Blocking the communication systems so the UAV can't receive enough or any signals
- Injection: Introduction of invalid, malicious data to gain control of the UAV or to affect its functions

The selection of appropriate security mechanisms is based on following criteria [Dao17]:

- Integrity: No package dropping, which means that the information sent complies with the information received
- Availability: The UAV can still operate and perform its functions despite being under attack
- Authenticity: Each node of the UAV network is able to detect the identity of the node with whom it communicates
- Confidentiality: Transferred data cannot be accessed by unauthorized parties

Choosing proper security mechanisms for UAVs, regarding the criteria mentioned above, leads to a dilemma: On one side an appropriate security system is requested and on the other side an almost real-time data transfer is needed. The security system must be robust with a high level of security and a low false-positive rate, light weight in terms of computing expenses and therefore it should have a low energy consumption. The security system used for HecTO-R is structured as follows:
In order to aggravate spoofing attacks the RAIM, which is already mentioned in chapter 4.8.1 and used in addition for navigation purposes, is used. As noted in chapter 4.8.1 RAIM excludes erroneous navigation signals which makes GPS spoofing more difficult. However it must be noted that an attacker can still spoof navigation signals when knowledge of the trajectory of a UAV is available [Sam14]. Since the UTM network and legislation of some countries stipulate that sensitive information like the position and velocity of a UAV is shared, this case is present. Thus, further security measures are required:
Rule-based detection methods recognize possible attackers on the basis of predetermined rules and patterns of real attacks. These detection algorithms are designed light weight and with a low false-positive rate. The included intrusion detection system (IDS) and intrusion prevention system (IPS) monitor anomalies in the signal strength intensity of GPS signals [Hic18]. Considering that many GPS spoofing attacks use high intensity erroneous signals it is highly possible to detect these kind of attacks. Nonetheless they are not robust enough because the predefined rules and patterns need to be updated in order to obtain a high level security [Hic17].
Whereas bio-inspired detection methods are based on light weight machine-learning algorithm and therefore show a good robustness. Yet these algorithms imply a higher false-positive rate and have also high computing expenses [Hic17]. Therefore it is intended that the computing of the algorithm takes place on the more powerful ground station and the computing results are transferred via encrypted telemetry messages to HecTO-R.
With the help of a hybrid detection method of rule-based and bio-inspired detection a high level security with a high detection rate and a low false-positive rate against spoofing and jamming attacks is given. To prevent injection attacks at sensitive data like ADS-B messages, they need to be equipped with End-to-End Encryption (E2EE) [Hic17]. Since an excessive use of encryption methods lead to a limitation of an almost real-time data transfer, only necessary systems which are not covered by the hybrid detection systems are considered.
The combination of all systems mentioned above generates a high level security and a high robustness by maintaining a low energy consumption and low false-positive rates with a minimum of cyber attack risks. Furthermore the used algorithms are intelligent enough to separate the GNSS signals from spoofed signals which is why a safe return-to-home function is possible [Art19].
Appropriate measures to occurring cyber attacks are further described in chapter 4.9.

4.8.5. Autopilot

As the most types of sensors (excl. camera) and the autopilot are build in Micro-Electro-Mechanical Systems (MEMS) design the overall weight and costs are low. Although the appearing impact of landing is almost zero due to HecTO-R's hovering, the avionic compartments are equipped with shock mounts to prevent any damage to the sensitive sensors.
The autopilot ensures that HecTO-R stays or gets into a stable mode, it guides HecTO-R to follow the trajectory specified by the operator or generated by the guidance system and it determines HecTO-R's coordinates for the navigation system. Therefore the autopilot is the centerpiece of the avionics and includes various subsystems [Sad20] as shown in figure 11.

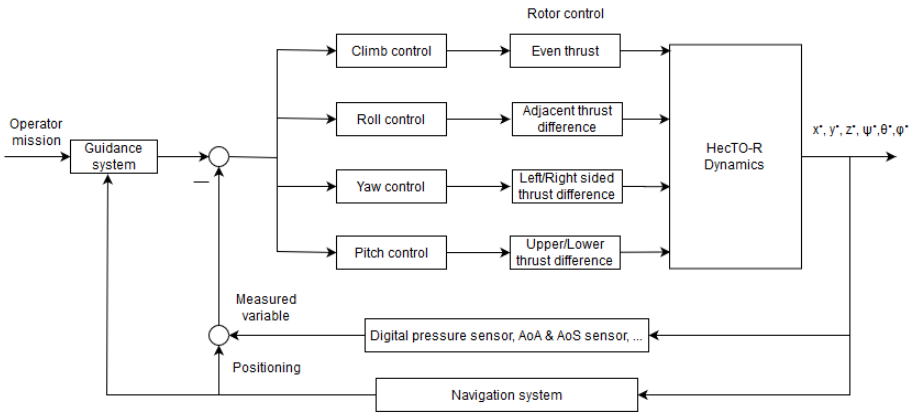

Figure 11: Flight control in HecTO-R

As shown in the aforementioned figure the guidance commands are the input for the control system where, depending on the active controller (described below) and the followed trajectory, the rotors are controlled accordingly. According to HecTO-R's dynamics the measuring instruments and the navigation system form the input for the guidance system via a closed loop control system.
Depending on the desired phase one of three different types of controllers is activated through input parameters like pitch angle, velocity, etc. These controllers can be divided into a cruise controller (where HecTO-R's aerodynamic behavior is comparable to a fixed wing air vehicle), a Take-off & Landing Controller (flight characteristic is comparable to a multicopter) and a transition controller (since these flight attitudes require different controlling) [al19b].
As an example for the T/O Transition (Phase 1), which is described in detail in chapter 5.2.4, the measuring instruments determine the time, velocity and the altitude of HecTO-R. The transition controller is activated and calculates the required pitch angle and thrust to follow the trajectory with the required radius R given by the guidance system. The remaining error between the current and the requested trajectory is reduced to zero by PID controlling.

Since some input parameters for the autopilot (e.g. GNSS, IMU, Camera, sensors) need to be digitalized, the autopilot contains an analog to digital (A/D) converter. The same applies to some output parameters from the autopilot (e.g. aileron servo, rotors) which need to be converted through a digital to analog (D/A) converter [Sad20]. Due to the expensive and time intensive design process of an own and individual autopilot, available autopilots such as the Pixhawk 4 [Tea20] can be used, which can also be easily extended as requested.

4.9. Emergency systems

The emergency systems implemented in HecTO-R guarantee both fail-operate and fail-safe features. The former property applies to software anomalies (e.g. spoofed GPS signals) whilst the latter applies to most hardware failures. With the help of 3D mapping algorithms HecTO-R detects potential emergency landing sites in case of various system failures. A return-to-base function is additionally included in the safety concept. Whilst locating the emergency landing spot, HecTO-R begins with the descent, using the undamaged, available propellers and/or ailerons to navigate towards the designated site. If all four propellers work, a conventional vertical landing is executed. If at least one is faulty the propellers are turned off once the height of 30 m is reached to prevent potential damage to property and injuries to people. Thereafter the UAV will glide down to the landing site.
Furthermore, Built-In Test Equipment (BITE) [God20b] is integrated in all avionic modules. For the error detection the BITE uses the monitoring method while being in the air. The data is then sent to the GCS and evaluated. In case of error the GCS finds countermeasures and is ready to repair the soft- or hardware failures.

5. Flight Performance

Flight performance calculations can be seen as the driving force behind an UAV's design. The UAV has to check or exceed all required performance values set by the design committee listed in section 2 and fulfill further requirements set by acting regulatory bodies e.g. Certification Specification CS23, which in some parts however, do not apply to that type of air vehicle due to the nature of the concept. Regulations still need to be established in the future. Some performance considerations are therefore merely assumptions based on acting regulatory frameworks.

5.1. Mass Estimation

A very complex topic regarding air vehicle sizing, having a somewhat good idea regarding mass is crucial for a successful design. For any type of efficient air vehicle it is important to reduce weight through an efficient use of structural optimization, lightweight materials (e.g. composites or lightweight metals), minimize wasted space and maximize useful space. Traditionally, this is done by using empirically estimated weight ratios wherever a weight is not yet known. Practically, this approach is used for the empty air vehicle frame and fuel sizing while other values (e.g. payload, electronics etc.) may already be known. In this case, it is especially difficult to estimate the right battery and engine weights as well as their respective sizes because these values depend on the overall air vehicle performance and need to be resized if performance calculations exceed estimations. The design does not require the fuel estimations for typical combustion engines since it makes use of an entirely electrified power train. This means that there is no variation in gross air vehicle weight during flight and the only changing factor is the payload. Overall, it is a process that runs through

many iterations and the use of spreadsheets and an organized management of all masses and their positions need to be tracked and dynamically adjusted for the right total loaded/unloaded CG position. therefore, two conditions need to be fulfilled:

- The CG of the unloaded air vehicle, meaning the weight of the entire air vehicle without the payload, needs to be at the correct static margin in front of NP
- If the payload is added, the position of the CG of the payload ideally needs to be at the same position as the CG of the unloaded air vehicle or the total loaded air vehicle CG only moves within static margin, allowing for fluids to be carried and the position of the payload could be placed further aft as well. Here, some trim through the use of differential thrust is needed but is only required during horizontal flight phases and can even be adjusted efficiently without using any additional energy in total.

The total loaded/unloaded air vehicle mass can be estimated as follows:

$$m_{max} = \frac{m_{Payload} + m_{Electronics} + m_{Parachute} + m_{Engines} + m_{Propellers}}{1 - (\frac{m_{BWE}}{m_{max}}) - (\frac{m_{Battery}}{m_{max}})} \tag{10}$$

With $(\frac{m_{BWE}}{m_{max}})$ and $(\frac{m_{Battery}}{m_{max}})$ being the mass ratios for the unloaded air vehicle frame and battery. m_{min} is then simply m_{max} with the payload subtracted from the value separately. While the ratio for the air vehicle frame follows traditional values for conventional air vehicle at ≈ 0.55 and lightweight air vehicle at ≤ 0.5, the battery ratio is strictly estimated and determined through many iterations as there are no general or applicable values for that ratio as of now. Approximation ratios and estimation methods are found in [Gol19] and [And10]. While these approximations all consider a conventional air vehicle layout there are simply no other estimation methods or weight ratios available.

5.2. Flight Phase Performance

5.2.1. Overview

To correctly estimate the performance needs of the air vehicle, all different flight phases during the span of one mission are being considered. This generally includes two types of flight scenarios that are assumed for each mission phase: constant velocity and accelerated/decelerated flight phases. The key values that need to be considered during all flight phases are the propeller thrust T and air vehicle velocity v since those values are key to establish all propeller and drive train power and energy needs.

5.2.2. General Propeller Sizing

For the necessary propeller power that needs to be available for a given air vehicle speed v and thrust T, the momentum theory or disc actuator theory is used. While it is not representative of a real propeller, it can be used for a first "ideal" propeller model of a propeller with disc area A_{Prop} and diameter $d_{Prop} = 700mm$ (28 inches) and propeller pitch of 20 inches which is smaller than pylon length $l_{Pylon} = 400mm$ to avoid contact between propellers or other aircraft parts. An added induction factor $k_{induced} \approx 1.25$ is introduced to try and model losses due to induced velocity. Further information can be found in [Phi09] and [al16]. However, real propeller calculations require the use of the blade element momentum theory since it combines all necessary propeller geometry and drag data and, most notably, the rotational speed and moment of the propeller. Here, comparing required thrust and airspeed of the design concept to existing propeller parameters and then choosing the correct propeller based on those values as well as requirements e.g. low-revs, low propeller shaft power at each phase for maximum efficiency, minimal noise production and energy consumption is the more approachable method. For now, the momentum theory is used. The required power of one propeller for a given true aircraft speed (TAS) v, thrust T and amount of propellers n_{Prop} is calculated as follows:

$$P_P(T, v) = k_{induced}(\frac{T}{n_{Prop}})[\frac{v}{2} + \sqrt{(\frac{v}{2})^2 + (\frac{\frac{T}{n_{Prop}}}{2A_{Prop}\rho})}] \tag{11}$$

A propeller that would provide the required performance for all phases is provided by APC Propellers. Its performance values are found in [Pro20] and produce the required thrust at given airspeeds throughout all phases while simultaneously matching up with the selected motors for correct power and RPM delivery. The total energy need of all propeller drive trains during all phases is the integral of the total propeller shaft power (as calculated in equation 11) over time divided by drive train efficiency $\eta = 0.81$ given in chapter 4.6.1 (for further details see [Gol19] and [al16]):

$$E_P = \frac{n_{Prop} \int P_P(T, v) dt}{\eta} \tag{12}$$

Having the required thrust, airspeed, power and energy needs allows for the correct sizing of the drive train and battery in chapter 4.6.3. Aircraft specifications and flight phase performance curves are given in the appendices D.

5.2.3. Accelerated Vertical Take-Off (Phase 0)

The T/O phase launches the mission and flight performance calculations. It is an accelerated flight phase that requires the air vehicle to achieve above stall speeds to perform a controlled maneuver in phase 1. Now, it is important to mention that this happens fully vertically. A traditional T/O would happen horizontally and would require a runway but this is not necessary for the design and therefore saves great amounts of space on the ground. This gives a lot more flexibility to where the air vehicle can land and only minimal to no landing area facilities are required.

Here, only the zero-lift drag D_0 of the air vehicle is considered due to the assumption that lift is still very small and starts acting once the air vehicle reaches above-stall speeds. While this is obviously not true in practice, it remains subject to further testing since lift at these small speeds depends highly on the Reynolds number and all lift assumptions that are made are only valid for above-stall speeds. It influences the trajectory of the air vehicle by applying a force which would move the air vehicle sideways. But since the air vehicle is in a vertical position at T/O and the lift term at this point is considered to be very small, the lift-induced drag term is also very small in comparison to the weight. Once the airspeed is above stall, differential thrust is used to control flight trajectory (see equation 6). Acceleration $a_{0,P0}$ is a fixed value that is selected in such a way to best fit phases 0 and 1 for least thrust, travel time, power and energy consumption while still achieving required clearance height and reaching above-stall velocity to go over to phase 1. The required thrust for the accelerated vertical T/O is calculated as follows:

$$T = W + D_0 + m \cdot a_{0,P0} \tag{13}$$

Also, the greater the acceleration at low speeds, the less sensitive the air vehicle generally becomes to gusts. This gives the velocity at each point:

$$v_{P0}(t) = a_{0,P0} \cdot t + v_{0,P0} \tag{14}$$

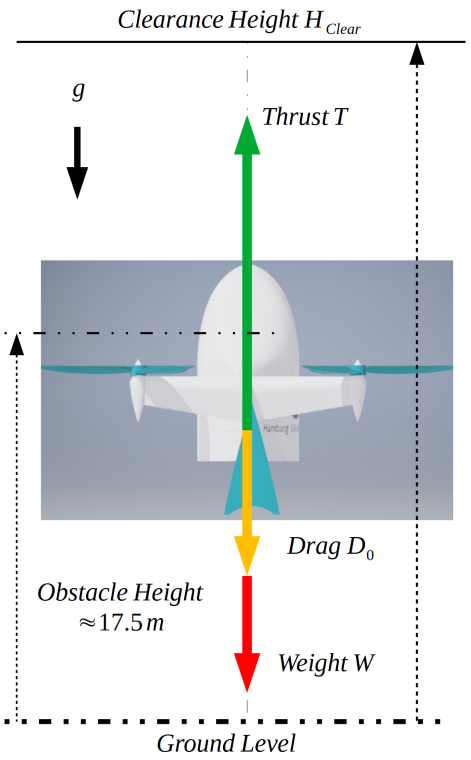

Figure 12: Accelerated vertical take-off (Phase 0)

with $v_{0,P0} = 0$ at start. Knowing the acceleration of the air vehicle the time t when it reaches a chosen clearance height H_{Clear}, which is set above the required obstacle height of $(17.5m > 50ft)$, is also known. Since initial velocity and altitude above ground AGL are zero, the vertical T/O time t is calculated as follows:

$$t = \sqrt{\frac{H_{Clear}}{0.5 a_{0,P0}}} \tag{15}$$

This concludes the performance calculations for phase 0 once clearance height H_{Clear} and an air vehicle speed $v_{P0} > v_{Stall}$ for phase 1 is reached (stalling speeds depend on flight configuration). All performance data for all phases are given in TLARD.

5.2.4. T/O Transition (Phase 1)

Having reached a sensible and at this point constant air vehicle velocity $v_{P1} = v_{P0} > v_{Stall}$ in vertical flight and having arrived at a height above obstacle and at clearance height H_{Clear}, the air vehicle now performs the transitioning from vertical to horizontal flight. Reaching above stall speeds in phase 0 is crucial for the assumptions of a linear lift coefficient slope to be both valid and the pitching moment be controllable by differential thrust. To estimate the required energy, the trajectory of the transition needs to be estimated. Here, a curved trajectory with fixed radius R is assumed which, ideally, is the difference between required

operating height and clearance height H_{Clear} in phase 0. However, R is limited by weight, altitude conditions and maximum lift coefficient $C_{L,max}$:

$$R \geq R_{min} = \frac{2 \cdot W}{\rho(ASL) \cdot g \cdot C_{L,max} \cdot S} \tag{16}$$

Therefore, clearance height H_{Clear} in phase 0 depends on minimum allowable radius and operational altitude between $120 - 150m$ while the air vehicle has to reach above-stall speed at this point as well and be above obstacle height. This maneuver follows the accelerated flight maneuver of a pull-up maneuver starting at 90° at constant air vehicle speed which is the entry speed v_{P1} once phase 0 is finished and phase 1 starts. The air vehicle now follows a curve with the fixed radius R and a constant initial airspeed v_{P1}, which gives us the fixed angular velocity. Staying on the curved trajectory requires a counteracting force pointing towards the center of the curve so that the flight path does not change. This is the centripetal force. Following formula shows the force equilibrium of the curved trajectory with radius R:

$$\frac{m \cdot {v_{P1}}^2}{R} = L - W \cdot cos(90° + \theta) \tag{17}$$

Following equations calculates the time in relation to initial conditions for a given pitch angle with $\theta_0 = 0$ as the initial pitch angle:

$$t(\theta) = \frac{(\theta - \theta_0)R}{v_{P1}} \tag{18}$$

Solving equation 17 for C_L gives the required lift coefficient for each pitch angle:

$$C_L = \frac{(\frac{m \cdot {v_{P1}}^2}{R} + W \cdot cos(90° + \theta))}{0.5 \cdot \rho(ASL) \cdot {v_{P1}}^2 \cdot S} \tag{19}$$

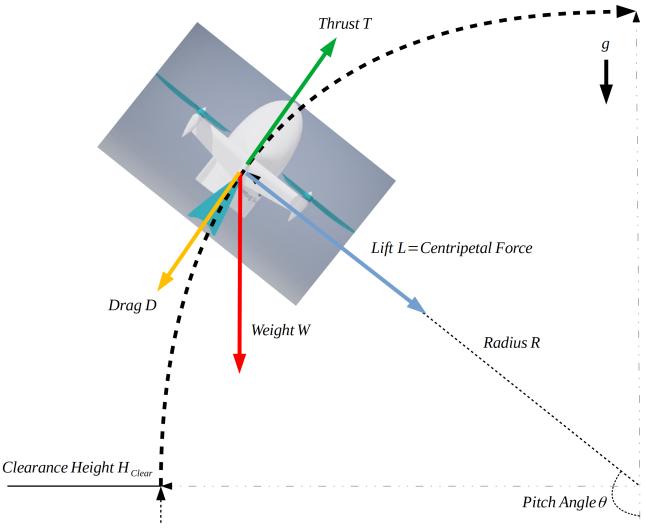

Figure 13: Depiction of the transitional T/O Maneuver (Phase 1)

Now, the issue with that maneuver is that the transition would result in an upside-down orientation of the air vehicle once horizontal flight is reached. To have the correct orientation once transition is performed, the air vehicle does not perform a pull-up maneuver but rather a push-down maneuver, meaning that it is actually pitching down from an initial vertical orientation and the resulting lift and lift coefficients are therefore negative, meaning the results in equation (19) need to be negated. This requires us to look at the other spectrum of the lift coefficient slope in figure 20 where it can been seen that the maximum negative stall coefficient $C_{L,max,neg} = -0.75$ is of a smaller magnitude than the positive counterpart $C_{L,max} = 1.2$, meaning that the reached velocity v_{P1} going into the transition needs to be even higher. This also means an increase in power output. For the push-down maneuver therefore an airspeed of $v_{P1} = v_{P0} > v_{Stall,neg} = 23.5 - 29m/s$ (depending on flight configuration and condition) is required. Here, peak propeller power of 20kW is reached. Another approach to solve this issue is by doing a roll maneuver once in horizontal flight. This is achieved by asymmetric aileron deflection and/or by inducing a rolling moment through adjacent differential thrust. To avoid such maneuvers the first approach is chosen for air vehicle safety reasons but both maneuvers can be performed. Having gathered all the information about the air vehicle motion the required thrust, propeller power (see equation 11) and battery energy (see equation 12) for the drive train can be calculated:

$$T = W \cdot cos(\theta) + D \tag{20}$$

With drag D now also including the lift-induced drag.
All in all, this maneuver is very complicated to perform and requires full pitch control for ever-changing conditions thus requiring very responsive, efficient and powerful propellers, motors, electronics and a sophisticated flight controller. To induce the necessary pitch-down moment for trajectory control further differential thrust or aileron input is required (see equation 6).

5.2.5. Cruise (Phase 2)

For a given altitude and weight configuration equation 7 gives the necessary cruise speed. Here, it is important to fulfill following factors for a safe and legal flight under design challenge and regulation requirements:

- In [Thi20], following equation provided by Certification Specification (CS) 25 is given to estimate required air vehicle cruise speed:

$$v_{Cruise}(\rho(ASL), W) \geq v_{Gust} + 43kts = 32.5\frac{m}{s} \tag{21}$$

With $v_{Gust} = 20kts$ as per design requirements. This requirement is met for all possible configurations at given $C_{L,Cruise}$ even though it applies for heavy commercial air vehicle. Therefore, the air vehicle is highly gust resistant during cruise since all cruise speeds are above $32.5\frac{m}{s} > 63kts$.

- Another important value is that cruise speed should be considerably higher than 1.2-1.3 times stall speeds for a given flight configuration. While these values are obviously taken from traditional start/-landing requirements as in [And10], they are crucial for the later evaluation of transitional maneuvers (T/O and landing) to further ensure a safe mission.

$$v_{Cruise}(\rho(ASL), W) > 1.3 \cdot v_{Stall}(\rho(ASL), W) = 1.3 \cdot \sqrt{\frac{2 \cdot W}{\rho(ASL) \cdot C_{L,max} \cdot S}} \tag{22}$$

With stall speeds being around 18.5 m/s for the unloaded air vehicle at 0 m ASL and 22.5 m/s for the loaded air vehicle at 3000m ASL. Here, stall requirements are also met when compared to cruise speeds in chapter 4.1.4. The pure horizontal flight time for one mission is then also known and exceeds the required time set by the design challenge.

The last crucial values for the cruise phase are the required thrust, power and battery energy calculations. Here, the cruise thrust can be calculated as in [Thi20]:

$$T_{Cruise} = D_{Cruise} = \frac{W}{(\frac{C_{L,Cruise}}{C_{D,Cruise}})} \tag{23}$$

With $\frac{C_{L,Cruise}}{C_{D,Cruise}}$ being the lift-to-drag ratio which for all cruise flight configurations and conditions is 23.3 since air vehicle trim happens by flying at slightly different airspeeds as mentioned before in chapter 4.1.4. Following equations (11) and (12) gives the required cruise performance values. An image of cruise flight is given in figure 2.

5.2.6. Landing Approach (Phase 3)

As the air vehicle approaches the landing platform, it needs to lose altitude and speed within the given distance of 1500 m and reach an altitude above or at obstacle height of 17.5 m > 15.24 m (50 ft) as required by the design challenge. To really optimize the landing approach, thrust needs to be reduced to, optimally, zero. However, since the approach happens at a rather steep approach angle $\gamma_{Approach}$, it most likely requires some reverse thrusting. With the selected motors and propellers, reverse thrusting is possible. For a chosen approach length $l_{Approach}$ and altitude difference as the difference between cruise and obstacle height $H_{Approach}$, the angle of approach $\gamma_{Approach}$ is calculated as follows:

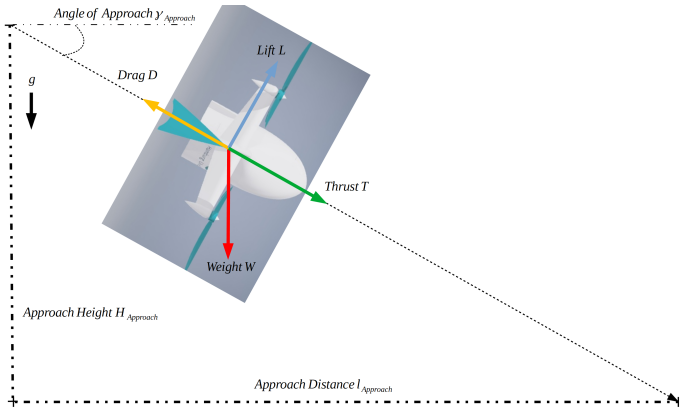

Figure 14: Depiction of landing approach (Phase 3)

$$\gamma_{Approach} = tan(\frac{-H_{Approach}}{l_{Approach}}) \tag{24}$$

The approach angle is slightly steeper than recommended at $-3°$ but within reasonable margin of $-6°$ to $-2°$. For the landing approach the air vehicle speed is required to be above stall speed. A constant airspeed at around $v_{P3} \approx 1.2 - 1.3 v_{Stall}$ is therefore chosen. The required lift coefficient and lift-to-drag ratio that needs to be upheld for the approach is then calculated:

$$C_{L,Approach} = \frac{W \cdot cos(-\gamma_{Approach})}{0.5 \cdot S \cdot \rho \cdot {v_{P3}}^2} \tag{25}$$

The required thrust is then calculated as follows:

$$T_{Approach} = W \cdot sin(\gamma_{Approach}) + D_{Approach} \tag{26}$$

5.2.7. Landing Transition (Phase 4)

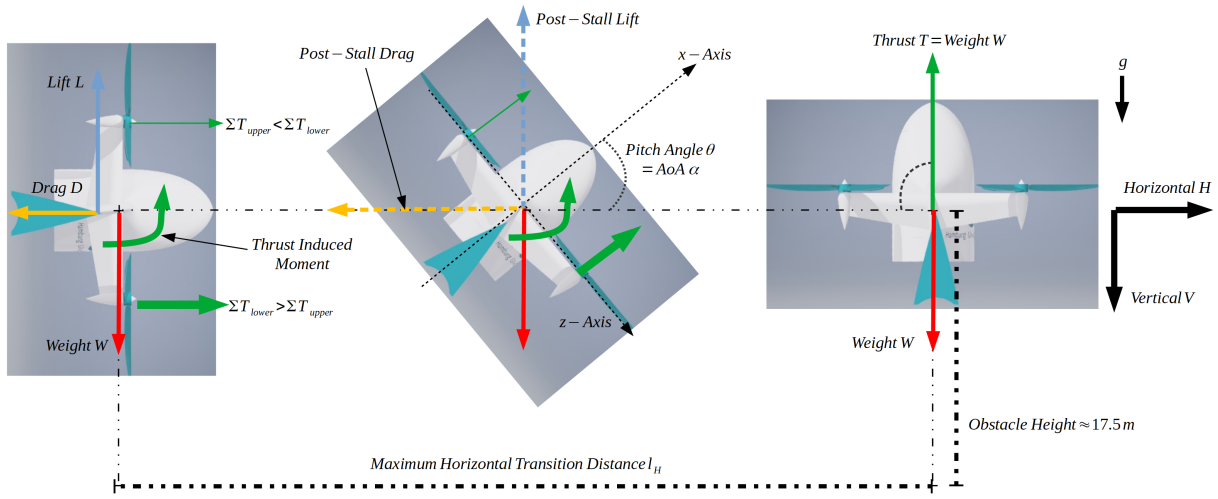

Figure 15: Depiction of landing transition (Phase 4)

Landing transition happens as shown in figure 15. It is a rotation around the air vehicle's y-Axis. This might seem similar to the T/O maneuver in phase 1 (see chapter 5.2.4) but it stands very much in contrast to it. In T/O the transition happens while flying a curved path with a transition radius R. Here, the altitude does not change and the air vehicle rotates directly around its y-Axis following a horizontal path. This can be viewed as an induced rotation of the air vehicle while T/O is more of a rotation due to a pull-up/push-down maneuver following a curved path. Here, it is necessary to take a clearer look at the pitching moment of the air vehicle as given in equation 6. Solving the equation for ΔT gives us the required difference in thrust between the upper and lower propellers of the air vehicle to induce the rotation for given moment of inertia I_{yy}, a reasonable pitch acceleration $\ddot{\theta}$ and all other given values in the equation which are established in chapter 4.1 and provided in figure 3. However, there are some things to mention before estimating transition parameters as this requires numerical solutions due to following challenges:

- Since the vertical position does not change to avoid a sudden increase/decrease in altitude to allow for a near-ground transition and therefore wanting to try and stay level during transition, with an increase in pitch θ the AoA automatically increases as well. In this case both angles are equal, meaning $\theta = \alpha$ due to the nature of the movement which is, as mentioned before, a strictly horizontal movement with a change in air vehicle pitch and therefore simultaneously in AoA. This basically means that once stall and post-stall AoA's are reached it is not permitted to use basic lift and drag assumptions as in horizontal flight to model the acting forces. However, knowing lift and drag is essential to correctly predict the further horizontal deceleration, differential thrust for the rotation and the air vehicle's overall motion and performance.

Since information regarding post-stall behavior of the air vehicle is yet to be determined, it is assumed that these forces do not act at all during landing transition. The vertical force equation is now the following:

$$ma_{V,P4} = \Sigma F_V = T \cdot sin(\theta) - W + [L_{Post-Stall}] \tag{27}$$

Ideally, $a_{V,P4} = 0$ and $v_{V,P4} = 0$ since the air vehicle shall not change position vertically to transition. Since post-stall behavior is unknown, this assumption cannot be upheld. Therefore, excluding lift, it can be calculated by how much the air vehicle would drop in altitude. Due to the pitch angle θ being very small at the beginning of landing transition the vertical forces cannot be equaled out efficiently, which finally causes a vertical acceleration towards ground meaning $a_{V,P4} \neq 0$. Provisionally, setting total thrust T to equal air vehicle weight W at transition start jerk is experienced, meaning that the acceleration towards ground changes. Simultaneously, the pitch angle θ changes due to the thrust-induced pitching moment $\Delta T \cdot l_{Pylon}$ of the propellers described in equation 6. This essentially results in a different thrust distribution between upper and lower propellers. It does not mean that reverse thrusting of the upper propellers is needed but simply a thrust difference between upper and lower propellers while in sum still equalling air vehicle weight. With an increase in pitch the drop distance is minimized as long as the transition itself is quick enough. This is achieved by the the high thrust capabilities of each propeller. Since the air vehicle also has a positive total zero-lift moment coefficient $C_{M0,tot}$ due to stability reasons the pull-up maneuver can be performed without reverse thrusting of the upper propellers. Again, the difference in thrust that is required between upper and lower propellers is

calculated using equation 6 and an efficient differential thrust distribution using equation 5 is chosen while total thrust T still remains equal to air vehicle weight W for hovering. Therefore, reverse thrusting is avoided. The horizontal force equilibrium can be written as follows:

$$ma_{H,P4} = \Sigma F_H = T \cdot cos(\theta) - [D_{Post-Stall}] \tag{28}$$

Here, the post-stall information regarding drag is also unknown, which in this regard is significant. The horizontal acceleration and speed of the air vehicle are calculated as if they are not affected by drag but purely by change of thrust in that direction, giving the maximum horizontal distance l_H during transition that the air vehicle would travel if drag wouldn't slow it down gradually. In reality, this distance would be much shorter due to the deceleration caused by drag. But for now, l_H can be added to the landing approach distance $l_{Approach}$ in phase 3, adding up to the total landing distance, which is shorter than the required 1500 m. This maneuver remains the only lesser known factor in the flight performance calculations since it cannot be evaluated using basic assumptions due to post-stall situations. These require the use of more sophisticated testing, validation, simulation and control methods as described in chapter 4.8.5. These methods determine exactly how the air vehicle behaves at such high AoA's and how to correctly, efficiently and safely execute all types of maneuvers, especially landing transition and adapting the air vehicle dynamics to each phase. The actual total power requirements may be much smaller though once post-stall lift and drag are known. While the differential thrust may need to be larger due to lift-induced pitching moment it is compensated by the simultaneous slow down of the air vehicle due to drag resulting in a reduction in overall lift and counteracting lift-induced pitching moment. The required differential thrust then becomes a function of the lift coefficient in regards to AoA in equation 6. Knowing post-stall lift also allows for a gradual approach to total thrust needs. Instead of assuming that it has to be equal to air vehicle weight W from transition start the amount of total thrust is increased ever so slightly in equation 27 so that the sum of all vertical forces remains 0. Now, as the air vehicle has transitioned from horizontal to vertical orientation, it goes into hover mode and makes the final landing descent.

5.2.8. Hover & Final Landing Descent (Phase 5)

Once the air vehicle has transitioned from horizontal to vertical flight mode and lost its entire air vehicle speed, the air vehicle needs to produce enough thrust to hover for a certain amount of time to even itself out and reach the correct landing position. This induces a propeller speed that in this case is not equal to the air vehicle speed but is the pure induced velocity produced by the propellers to generate the required thrust, which needs to be equal to weight (T=W). Per propeller this equates to:

$$v_{induced,P5} = \sqrt{\frac{\frac{W}{n_{Prop}}}{2\rho A_{Prop}}} \tag{29}$$

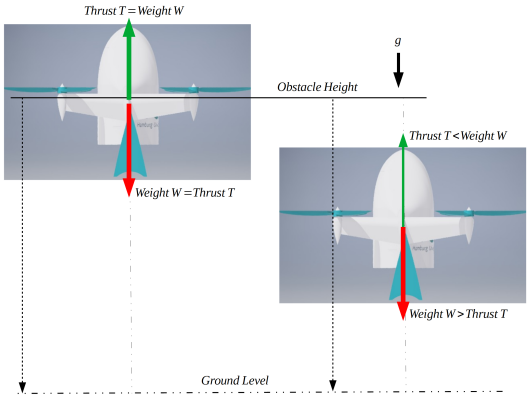

Figure 16: Depiction of final landing hover and descent (Phase 5)

The resulting propeller power is then estimated using the same approach as in equation 11 with the actual airspeed $v = 0$ since the air vehicle is hovering. This calculates the induced power per propeller for hover. Depending on how long hover time is the total hover energy is calculated using equation 12. For this phase a conservative value of around 30 seconds hover time is selected. The final landing descent happens in a similar fashion to a quadcopter. Subtracting the required descent velocity, which is chosen conservatively at around $1 - 2m/s$, from the induced velocity at hover gives us the new, smaller induced velocity of the propellers by the amount of the descent velocity chosen before, creating a power and, retrospectively, a thrust reduction. The final landing still requires testing and simulations as to how the landing is approached to reduce landing impact and sensitivity to gusts or any side effects since the air vehicle is technically flying "backwards", optimizing the procedure for a fast and secure landing. This is generally done by rotating the air vehicle at hover so that when there are side winds the flying wing is oriented so that the cross sectional surface in wind direction is minimal. Additionally, the propellers keep the air vehicle from rocking around aggressively similar to a quadcopter.
The final descent of the air vehicle, the safe landing and engine shutoff conclude the raw flight phase performance evaluation and calculation.
The approximated power, thrust and air vehicle velocity graphs for the most extreme flight configurations are shown in the appendices D. Figure 27 displays the most power-intensive yet shortest flight for a fully loaded air vehicle at 3000m ASL while figure 28 the most power efficient yet longest flight for an unloaded air vehicle

at 0m ASL. It is clearly visible in the graphs that the most power-intensive phases are the transition phases. This is due to the fact that the air vehicle thrust vector is vertical to the weight vector which significantly increases propeller power needs for T/O and landing. Lowest power phases include both cruise and landing approach as expected. The final air vehicle performance specifications are given in the appendices table 8.

6. Operations & Costs

6.1. Costs

HecTO-R is able to start from a platform which is equipped with the loading robot called Roll-E and a GCS for monitoring and battery changing purposes. The package landing and unloading can be executed wherever it is needed and without the help of e.g. a Roll-E. Even though it is intended that the package is delivered to a specific landing platform, HecTO-R is even able to deliver e.g. to the customer's backyard.
As described in chapter 4.5.1.3 HecTO-R's and Roll-E's batteries are changed at the base. Below a business scenario in the United States is considered, since the UTM network is implemented there and regulations (e.g. air carrier certification) are researched from the corresponding authority FAA. Still, the business scenario is also suitable for Germany due to high similarities (e.g. between regulations by EASA and FAA).

In the following chapters the maximum workload, which means 24 hours operations or 29 missions per day for each HecTO-R is considered. To meet the requirements of 0,5 missions per minute (described in the TLARD under R2.14) and at the same time having reserve, 7 HecTO-Rs and 3 Roll-Es are needed. 24 hour operations can only be done with corresponding precautions (e.g. lightings, reserve fleet, additional employees). Furthermore the longest and the shortest flight durations are considered in order to present a price span.

6.1.1. Non-Recurring Costs

The empty weight cost of HecTO-R can be estimated through the average air vehicle costs per weight [Val05][al05]. In [al05] a rough estimation for Department of Defense (DoD) UAVs is presented. The formula is based on heuristic and rule of thumb and fits also for HecTO-R, since the UAVs mentioned in [al05] are in a similar category of speed and weight. Using the formula 1350 € per lbs the empty weight cost, which includes material, production and developing costs, can be estimated to approximately 70.200 €. Adding the remaining costs described in the TLARD in figure 2 an approximated total cost for one HecTO-R of 80.800 € can be obtained. The costs of one Roll-E were calculated through the used parts and estimated production costs to 800 €. That leads to total purchase costs of 586.000 € for 7 HecTO-Rs and 3 Roll-Es.
The lifespan for HecTO-R and Roll-E is estimated to 5 years [Hut16] and those of the batteries amounts to 1000 cycles. Regarding these factors and considering that 60 km mission (2 missions) are 2,97 - 3,4% of a day (described in figure 30), HecTO-R's & Roll-E's total costs of 10,64 - 12,02 € per 60 km missions are obtained. The reference of 2 missions or 60 km is chosen since the battery change time is only considered after the second mission.
Since HecTO-R weighs more than 55 pounds, it does not fit to the requirements of FAA Part 107. Nonetheless the FAA published Part 135 for air package delivery certification beyond visual line of sight (BVLOS) which requires an airspace authorization and a standard air carrier certification. To get the former authorization a request to the responsible USS or the Low Altitude Authorization and Notification Capability (LAANC) is necessary. The latter needs to be done when flights near protected area e.g. airports is desired. The standard air carrier certification is necessary since the operator needs 7 HecTO-Rs and 3 Roll-Es to meet the requirement of 0,5 mission starts per minute and to have an additional reserve. The mission duration used are listed in the TLARD shown in figure 2. The process for a Part 135 certification is described in chapter E.1 in figure 29. The process may take several years and the costs for the certification vary depending on e.g. the size of the fleet. According to [USA20] the costs for the air carrier certification for Part 135 may amount to approximately 40.000 €.

For estimating the costs for the GCS the data of the MQ-9's GCS is considered which amounts to 2,8 Mio. € [Get15]. As the complexity of HecTO-R and its mission is comparatively lower it can be expected that the costs for a GCS will also be lower. The GCS's costs for HecTO-R's purposes can be estimated to a quarter of the aforementioned military GCS, which then amounts to 0,7 Mio. €. Considering a time span of five years, due to any software and hardware updates needed, the ownership costs for the used GCS amounts to 11,39 - 13,04 € per 60 km. Adding this result with the costs for the aforementioned ownership of the 7 HecTO-Rs and 3 Roll-Es, the total ownership costs of 22,03 - 25,06 € are obtained.
The energy consumption of the GCS can only be compared with other GCS [Pik97] and estimated to round about 15.000 kWh per year. With the current costs for renewable energy in the US with (0,03 €) per kWh

[Mar20] the approximated annual energy costs of 450 € can be obtained, which leads to 0,037 - 0,042 € per 60 km.

6.1.2. Recurring Costs

Using the described formula [DAn14] for obtaining the energy costs per kilometer and HecTO-R's parameters results to:

$$\frac{c_{el}}{e_{eff}} * (\frac{m_p + m_v}{370 * \eta_{transfer} * r} + \frac{p}{v_{Cruise}}) \tag{30}$$

The used abbreviations and the values can be looked up in the nomenclature and in the chapters 5.2.5, 4.6.3 & 4.6.1. The result is the average cost for the energy per kilometer with 0,0038 - 0,0046 €/km. This result seems ultra low but is not surprising since the properties of modern batteries e.g. the efficiency are improving continuously. It can be expected that these properties will improve even more in the next few years.

With the data calculated above costs of 0,23 - 0,28 € per 60 km for one HecTO-R until battery changing are obtained, which therefore amounts to 1,61 - 1,96 € per 60 km for 7 HecTO-Rs. Since Roll-E's battery has a power consumption of 0,45 Wh, 0,04 € per hour which means 30 missions for one Roll-E until battery changing is obtained. In order to reference the data to HecTO-R's 60 km missions the energy costs for 3 Roll-Es amount to approximately 0,028 - 0,03 € with 1 min work time for each Roll-E. In summary energy costs for 60 km missions (2 missions) of round about 1,64 - 1,99 € are obtained.
The maintenance costs of HecTO-R are estimated using Hemingway's iceberg theory [Baj18] and experience values from [Cha17] to approximately 50% of the purchase costs so that the maintenance costs amount to 4,76 - 5,46 € per 60 km.

Although HecTO-R and Roll-E are autonomous the operator needs staff for monitoring and maintenance purposes. The maintenance includes the replacing of the batteries and in addition to that other needs of maintenance is monitored and transmitted by the Built-In Test Equipment (BITE) as described in chapter 4.9. The annual costs for a director of maintenance and a director of operations may be estimated each to 45.000 - 75.000 € [Kan14][pay20].
In addition staff for the logistic is needed whose amount is estimated to 3 and whose annual salary is estimated to 30.000 € [ind20]. Offering 24 hour operations the employees need to work in shifts, which makes a minimum number of 2 manager for each task necessary. This leads to total, annual staff costs of 270.000 € and therefore referred to 60 km missions costs of 21,97 - 25,15 € are obtained.
Furthermore several insurances for HecTO-R, Roll-E and the ground station are recommended. The following insurances could be taken into consideration: Drone liability coverage (includes property damages and injuries caused by HecTO-R), Drone hull coverage (includes damages to HecTO-R), Onboard components coverage (includes damages to HecTO-R's onboard equipment e.g. camera), Ground equipment coverage (includes damages to ground equipment e.g. GCS) [Hun20]. The costs for the insurance is linearly approximated using the DJI Phantom 4's data. The drone weighs approximately 1,4 kg with annual insurance costs of approximately 670 € [Nix20]. Considering HecTO-R's weight the estimated annual insurance costs for 7 HecTO-Rs are approximately 87.100 € which lead to 7,09 - 8,11 € for 60 km missions.

6.2. (In-)Direct Operating Costs (IOC & DOC)

By adding up all the necessary costs mentioned above, the direct and indirect operating costs are obtained, which are shown in chapter E.1 figure 31. As the costs are referred to 60 km and therefore 2 missions, one single mission delivery has DOC of 3,20 - 3,73 € and IOC of 25,56 - 29,18 €.

6.3. Rough Market Analysis & Business Case

As described in chapter 6.1 HecTO-R's concept offers the opportunity to operate in a 24 hours network plan. This and the short delivery time lead to a differentiation from the competitors like Amazon Prime Air or DHL Drone Delivery. The mentioned competitors are also incapable of operating drones with a MTOW higher than 5kg, since they are only able to operate in visual line of sight (VOL) [Bih18]. In addition there are several reports of competitor's drones colliding with trees and buildings due to wind. Based on HecTO-R's concept as a hybrid of a quadcopter and tailsitter in a blended wing configuration and due to its high developed avionic systems (e.g. detect-and-avoid, security system) it is less vulnerable and more stable in cruise.
As HecTO-R is monitored and tracked anyway, a package tracking service can be offered to the customers which is also helpful for potential theft attempts after previous emergency landings. Delivering to landing

platforms, which are optionally equipped with Roll-Es, a return of delivered packages is easy to achieve and makes the flight process even more effective while halving the costs.

The growing demand for online orders especially during the corona crisis requires a reliable, eco-friendly, express delivery. HecTO-R stands out with its high cruise speeds and therefore short delivery times. As shown in the TLARD (figure 2) under R2 HecTO-R's delivery time is 1,7 times shorter than required. Due to its full electric and green energy powered propulsion systems HecTO-R represents a serious competitor to conventional providers. Therefore the targeted customer segments are the following:

- Replacement parts delivery for specific industries (e.g. automotive industries), where long delivery times and delays lead to high costs for the production
- Medicine delivery to hospitals, pharmacies and private customers
- Crisis regions, which are hardly accessible via conventional routes
- Warehouse companies (e.g. Zalando) to cut out the outsourced delivery service providers (e.g. DHL, UPS)
- Express delivery in general, wherever short delivery times are needed

To provide a more in-depth example case from the above mentioned, HecTO-R's comparatively short delivery time is advantageous for the transport of vital organs or life-saving medicine to hospitals. Furthermore, the ongoing COVID-19 pandemic displayed a great demand of express delivery of protective equipment. Competitors such as Medlife [USA18] are offering express delivery within 2 hours, which takes 10 times longer than HecTO-R, since the UAV only needs 11,39 min to its destination. The other competitors like Amazon Prime Air operate also with a lower velocity in the amount of approximately 89 km/h [Dre15] which is lower than HecTO-R.
In conclusion the HecTO-R concept provides a diversified market segment and can convince with his fast and expandable offer.

7. Conclusion

The goal of the Joint NASA/DLR Aeronautics Design Challenge was to design a safe, reliable, secure, profitable and quite unmanned aerial system. HecTO-R can fulfill these requirements and desires with the use of redundant and latest technology combined with an expandable and unique business case.
The UAV is mainly made up of CFRP which makes it lightweight and simultaneously robust. The VTOL capability allows HecTO-R to take off and land independently of big platforms. The hybrid design between a blended wing tailsitter and a quadcopter enables short flight missions and also possesses good gliding properties.
Four larger and therefore quieter propellers powered by Licerion's latest battery technology generate enough thrust to fulfill 2 missions with a total distance of 60 km. The batteries for HecTO-R and Roll-E are recharged at the GCS with renewable energy which ensures emission free transportation. Furthermore, the installed noise protection walls on the starting platforms lead to lower noise emissions. For aerodynamic and redundancy purposes two ailerons are used which ensure flight control even in emergency situations. The electrically powered landing stilts round off the full electric unmanned aerial system. With the help of small, autonomous operating loading robots called Roll-Es the loading process is completed. HecTO-R is able to autonomously unload the package given that a flat surface is landed upon, which could enable landing regardless of any particular platform.
Due to HecTO-R's design the cruise flight is highly efficient since its gliding properties makes longer ranged flight missions with corresponding precautions (e.g. higher battery capacity) possible. As mentioned in chapter 6.3 the high UAV's velocity makes faster deliveries possible, outperforming competitors such as Amazon Prime Air. In addition HecTO-R is designed to get the needed certifications mentioned in chapter 6.1.1, so that BVLOS missions are possible and authorized.
The implemented avionic modules are designed with necessary redundancy and with the latest technology such as hybrid security algorithms. Therefore HecTO-R has great abilities regarding reliable detect-and-avoid, high situational awareness and a high security level.
The DOC of 3,20 - 3,73 € per mission and the fast delivery time makes an UAS of HecTO-Rs competitive in comparison to competitors or other conventional delivery providers.
By increasing the effort in flight dynamic tests more precise data for HecTO-R's aerodynamic behavior can be obtained. Further cost savings could be achieved through economies of scale.

References

[Ada18] Wiktor Klimek Adam Dlugosz. *The Optimal Design of UAV Wing Structure*. Institute of Computational Mechanics and Engineering, Silesian University of Technology, 2018.

[al05] Stephen A. Cambone et. al. *Unmanned Aircraft Systems Roadmap*. Office of the Secretary of Defense, 2005.

[al16] Bo Wang et al. *Preliminary Design of a Small Unmanned Battery Powered Tailsitter*. Hindawi Publishing Corp., 2016.

[al19a] Chaoyang Jiang et. al. *Experimental Investigation of Novel Porous-serrated Treatments on Airfoil Trailing Edge Noise Reduction*. Chaoyang Jiang et. al., 2019.

[al19b] Dibya Kanti Golui et. al. *Detailed Design of a Tail-Sitter*. Indian Tnstitute of Space Science and Technology, Department of Aerospace Engineering, 2019.

[al19c] Paolo Candeloro et. al. *Small-Scale Rotor Aeroacoustics for Drone Propulsion: A Review of Noise Sources and Control Strategies*. Paolo Candeloro et. al., 2019.

[al19d] Timothy Brungart et. al. *The reduction of quadcopter propeller noise*. Noise Control Engineering Journal, 2019.

[al20] Pamela Whitley et al. "UTM Concept of Operations v2.0". In: Federal Aviation Administration, 2020. Chap. 2.3.

[And10] John D. Anderson. *Aircraft Performance and Design*. TATA McGraw-Hill, 2010.

[Art19] Menaka Pushpa Arthur. *Detecting Signal Spoofing and Jamming Attacks in UAV Networks using a Lightweight IDS*. St.Joseph's Institute of Technology, 2019.

[Baj18] Umeshi Bajagain. *The incorporation of Hemingway's Iceberg theory in texts - a methodical approach*. Tribhuvan University, 2018.

[Bal20] Mike Ball. *High Energy Batteries Tested for HAPS UAV Applications*. 2020. URL: https://www.unmannedsystemstechnology.com/2020/05/high-energy-batteries-tested-for-haps-uav-applications/ (visited on 07/02/2020).

[Bih18] Corinna Bihler. *Fliegende Lieferanten: Wann setzen sich Lieferdrohnen im E-Commerce durch?* 2018. URL: https://parcellab.com/blog/logistik/fliegende-lieferanten-wann-setzen-sich-lieferdrohnen-im-e-commerce-durch/ (visited on 07/01/2020).

[Bla+12] Bradley F. Blackwell et al. *Exploiting avian vision with aircraft lighting to reduce bird strikes*. Journal of Applied Ecology, 2012.

[Bry12] Benjamin J. Tran Bryan W. Harris. *Fiber optic AFDX for flight control*. Bryan W. Harris, Benjamin J. Tran, 2012.

[Cha17] Andrew Chapman. *Drones: Total Cost of Ownership (TCO)*. 2017. URL: https://www.auav.com.au/articles/drones-total-cost-ownership-tco/ (visited on 07/01/2020).

[Cor20] Sion Power Corporation. *Sion Power's Licerion High Energy (HE) Technology Provides Impressive Performance in HAPS Application*. 2020. URL: https://www.prnewswire.com/news-releases/sion-powers-licerion-high-energy-he-technology-provides-impressive-performance-in-haps-application-301062696.html (visited on 07/02/2020).

[DAn14] Raffaello D'Andrea. *Guest EditorialCan Drones Deliver?* Raffaello D'Andrea, 2014.

[Dao17] Mohsen Guizani Daojing He Sammy Chan. *Communication Security of Unmanned Aerial Vehicles*. IEEE Wireless Communications, 2017.

[Dep19] André Deperrois. *Theoretical limitations and shortcomings of XFLR5*. 2019. URL: http://www.xflr5.tech/docs/Part%20IV:%20Limitations.pdf.

[Dir20a] KDE Direct. *KDE-UAS125UVC-HE*. 2020. URL: https://www.kdedirect.com/collections/uas-multi-rotor-electronics/products/kde-uas125uvc-he (visited on 07/02/2020).

[Dir20b] KDE Direct. *KDE8218XF-120*. 2020. URL: https://www.kdedirect.com/collections/uas-multi-rotor-brushless-motors/products/kde8218xf-120 (visited on 07/02/2020).

[Dre15] Frederic Lardinois Drew Olanoff. *Amazon Shows Off New Prime Air Drone With Hybrid Design*. 2015. URL: https://techcrunch.com/2015/11/29/amazon-shows-off-new-prime-air-drone-with-hybrid-design/ (visited on 07/01/2020).

[FAA18] FAA. *Aircraft Noise Issues*. 2018. URL: https://www.faa.gov/about/office_org/headquarters_offices/apl/noise_emissions/airport_aircraft_noise_issues/ (visited on 07/02/2020).

[Fer+11] Esteban Fernández-Juricic et al. *Bird strikes and aircraft fuselage color: a correlational study.* University of Nebraska - Lincoln, 2011.

[Get15] Dan Gettinger. *Drone Spending: the MQ-9 Reaper.* 2015. URL: https://dronecenter.bard.edu/drone-spending-the-mq-9-reaper/ (visited on 06/30/2020).

[Gie05] Christian Giesecke. *Nachtflugbeschränkungen und Luftverkehrsrecht : Luftverkehr im Spannungsfeld von Wirtschaft und Gesundheit.* Carl Heymanns, 2005.

[GKa90] Rudolf E. Großkopf et al. "Mustererkennung 1990". In: Springer Verlag, 1990. Chap. Ein robustes Verfahren zur Detektion und Verfolgung bewegter Pbjekte in Bildfolgen.

[God20a] Ralf God. *Flugzeug-Kabinensysteme.* Institut für Flugzeugkabinensysteme, TUHH, 2020.

[God20b] Ralf God. "Systems Engineering". In: Institut für Flugzeugkabinensysteme, TUHH, 2020. Chap. Fehlertoleranz.

[Gol19] Volker Gollnick. *Luftfahrzeugentwurf I + II, Lecture Notes.* Institut für Lufttransportsysteme, TUHH, 2019.

[Gol20] Volker Gollnick. "Methoden des Luftfahrzeugentwurfs II". In: Institut für Lufttransportsysteme, TUHH, 2020. Chap. 3.7.

[gre20] greencarcongress. *Sion Power projects Licerion EV Li-metal batteries will have 420 Wh/kg and 700 Wh/L when scaled to commercial design.* 2020. URL: https:/www.greencarcongress.com/2020/03/20200315-sion.html (visited on 03/15/2020).

[Gud16a] Snorri Gudmundsson. "General Aviation Aircraft Design: Applied Methods and Procedures". In: Butterworth-Heinemann, 2016. Chap. 9.2.

[Gud16b] Snorri Gudmundsson. "General Aviation Aircraft Design: Applied Methods and Procedures". In: Butterworth-Heinemann, 2016. Chap. 9.5.6.

[Gud16c] Snorri Gudmundsson. "General Aviation Aircraft Design: Applied Methods and Procedures". In: Butterworth-Heinemann, 2016. Chap. 9.5.10.

[Gud16d] Snorri Gudmundsson. "General Aviation Aircraft Design: Applied Methods and Procedures". In: Butterworth-Heinemann, 2016. Chap. 9.3.5.

[Hep18] Martin Hepperle. *Airfoil Design for Light Tailless Airplanes.* 2018. URL: https://www.mh-aerotools.de/airfoils/nf_8.htm (visited on 07/02/2020).

[Hic17] Nirwan Ansari Hichem Sedjelmaci Sidi Mohammed Senouci. *A Hierarchical Detection and Response System to Enhance Security Against Lethal Cyber-Attacks in UAV Networks.* IEEE Transactions on Systems, Man, and Cybernetics: Systems, 2017.

[Hic18] Sidi Mohamed Senouci Hichem Sedjelmaci. *Cyber security methods for aerial vehicle networks: taxonomy, challenges and solution.* Springer Science+Business Media, 2018.

[Hun20] Jessica Huneck. *Commercial Drone Insurance.* 2020. URL: https://www.trustedchoice.com/professional-liability-insurance/pilot-coverage/commercial-drone-insurance/ (visited on 06/30/2020).

[Hut16] Adrienne Welch Sudbury & E. Bruce Hutchinson. *A cost analysis of Amazon Prime Air drone delivery.* Journal for economic educators, 2016.

[ind20] indeed. *Logistics Associate Salaries in the United States.* 2020. URL: https://www.indeed.com/salaries/logistics-associate-Salaries (visited on 07/01/2020).

[Kan14] Dean Kantis. *Purchasing an Existing Part 121, 135, or 145 Certificate: Part 2 – Steps in Purchasing or Applying for a Certificate.* 2014. URL: https://www.universalweather.com/blog/purchasing-an-existing-part-121-135-or-145-certificate-part-2-steps-in-purchasing-or-applying-for-a-certificate/ (visited on 06/30/2020).

[Kon18] M. Lee & K. Kong. *Fourier-Series-Based Phase Delay Compensation of Brushless DC Motor Systems.* IEEE Transactions on Power Electronics, 2018.

[Kop17] David Koppel. *Why are there so many avionics communications specifications?* 2017. URL: https://www.mil-1553.com/why-many-avionics-communications-specifications (visited on 06/23/2020).

[Mar20] Silvio Marcacci. *Plunging Renewable Energy Prices Mean U.S. Can Hit 90% Clean Electricity By 2035 - At No Extra Cost.* 2020. URL: https://www.forbes.com/sites/energyinnovation/2020/06/09/plunging-renewable-energy-prices-mean-us-can-hit-90-clean-electricity-by-2035at-no-extra-cost/#61bf460a2f9b (visited on 07/11/2020).

[Mül20] Markus Müller. *eCalc*. 2020. URL: https://www.ecalc.ch/index.htm (visited on 07/13/2020).

[Nix20] Andrew Nixon. *How Much Does a Drone Insurance Cost? (2020 Update)*. 2020. URL: https://bestdroneforthejob.com/blog/drone-insurance-cost/ (visited on 06/30/2020).

[pay20] payscale. *Logistics Associate Salaries in the United States*. 2020. URL: https://www.payscale.com/research/US/Job=Maintenance_Manager/Salary (visited on 07/01/2020).

[Phi09] Warren P. Phillips. "Mechanics of Flight". In: John Wiley and Sons, Ltd., 2009. Chap. 2.4.

[Pik97] John Pike. *UAV Ground Control Station (GCS)*. 1997. URL: https://fas.org/irp/program/collect/uav_gcs.htm (visited on 06/30/2020).

[Pow20a] Sion Power. *Information Brief*. 2020. URL: http://sionpower.com/files/IB_Li-S2Licerion.pdf (visited on 07/08/2020).

[Pow20b] Sion Power. *Licerion*. 2020. URL: https://sionpower.com/products/ (visited on 07/02/2020).

[Pro20] APC Propellers. *28 x 20 Inch Propeller*. 2020. URL: https://www.apcprop.com/files/PER3_28x20-4.dat (visited on 07/02/2020).

[RW92] Daniel P. Raymer et al. *Aircraft Design: A Conceptual Approach*. AIAA Inc., 1992.

[Sad20] Dr. Mohammad H. Sadraey. *Design of Unmanned Aerial Systems*. John Wiley & Sons Ltd, 2020.

[Sam14] et.al. Samer Khanafseh. *GPS Spoofing Detection using RAIM with INS Coupling*. Illinois Institute of Technology, 2014.

[Sch15a] Dieter Scholz. *Aircraft Design, Lecture Notes*. Hamburg University of Applied Science, 2015.

[Sch15b] Dieter Scholz. "Aircraft Design, Lecture Notes". In: Hamburg University of Applied Science, 2015. Chap. 11.2.

[Stü20] Jürgen Stüber. *China drückt bei der Entwicklung von Lieferdrohnen aufs Tempo*. 2020. URL: https://www.gruenderszene.de/automotive-mobility/china-drohnen-logistik?interstitial (visited on 07/14/2020).

[Tea20] PX4 Dev Team. *Pixhawk 4*. 2020. URL: https://docs.px4.io/v1.9.0/en/flight_controller/pixhawk4.html (visited on 07/02/2020).

[Thi20] Frank Thielecke. *Grundlagen der Flugzeugsysteme, Lecture Notes*. Instiut für Flugzeugsystemtechnik, TUHH, 2020.

[TSt+08] T.Strang et al. *Lokalisierungsverfahren*. Deutsches Zentrum für Luft- und Raumfahrt, 2008.

[Umw20] Amt für Umweltschutz. *Maßnahmen zur Minderung der Lärmimmission*. 2020. URL: https://www.leipzig.de/umwelt-und-verkehr/luft-und-laerm/laermschutz/laermminderung/ (visited on 07/13/2020).

[USA18] USAC. *Medlife Express Delivery: Doorstep Delivery of Medicines in Just 2 Hours*. 2018. URL: https://www.medlife.com/blog/medlife-express-delivery-doorstep-delivery-medicines-just-2-hours/ (visited on 07/01/2020).

[USA20] USAC. *Air Carrier Certification*. 2020. URL: https://usac.com/faa/Price.asp (visited on 06/30/2020).

[Val05] Ricardo Valerdi. *Cost Metrics for Unmanned Aerial Vehicles*. Massachusetts Institute of Technology, 2005.

[Wet20] Wind Wet. *Airfoil Tools*. 2020. URL: http://www.airfoiltools.com/ (visited on 06/02/2020).

List of Figures

Appendices

A. Top Level Aircraft Requirements Document (TLARD)

No.	Description/Name of requirement	Term	Value (with tolerance)					unit (phys.)	Type of requirement
R			min.	exact	max.	HecTO-R	Amazon Prime Air [Dre15]		
1	**Geometry**								
1.1	UAV-Height					891,00		mm	Request
1.2	UAV-Width					2.756,00	914,00	mm	Request
1.3	UAV-Depth					1.477,00		mm	Request
1.4	Package Loading Height above ground			150,00		395,00		mm	Requirement
1.5	Package-Width			150,00		150,00		mm	Requirement
1.6	Package-Depth			150,00		150,00		mm	Requirement
1.7	Base size					89,67		m^2	Request
1.8	Landing platform size		7,00		112,50	93,50		m^2	Requirement
1.9	Landing platform height above sea level		0,00		2.500,00	2.500,00		m	Requirement
1.10	Avionics	Main, Left, Right Avionics Bay				0,02136		m^3	Requirement
1.11	Camera Geometry			60 (W) x 60 (L) x 105 (D)		60 (W) x 60 (L) x 105 (D)		mm	Request
2	**Mission**								
2.1	Cruise speed		12,50			35,00 - 42,00	22,36	m/s	Requirement
2.2	Cruise altitude		120,00		150,00	120,00 - 150,00	< 150,00	m	Requirement
2.3	Cruise route				15,00	15,00	16,00	km	Requirement
2.4	Take Off Distance				1.500,00	90,00		m	Requirement
2.5	Landing Distance				1.500,00	1.325,00		m	Requirement
2.6	Total Flight duration (One-Way)	Depends on flight conditions			20,00	9,00 - 10,60	30,00	min	Requirement
2.7	Mission frequency			0,50		0,50		Mission starts/d	Requirement
2.8	Lowering loading mechanism duration					20,00		s	Request
2.9	Loading duration by Roll-E					10,00		s	Request
2.10	Raising loading mechanism duration					20,00		s	Request
2.11	Locking loading mechanism duration					5,00		s	Request
2.12	Unloading duration by HecTO-R					40,00		s	Request
2.13	Loading duration	total				1,00		min	Request
2.14	Unloading duration	total				1,50		min	Request
2.15	Roll-E proceeding time					0,17		min	Request
	Total Delivery Time (Bidirectional)	Depends on flight conditions			40,00	20,50 - 23,70	> 60,00	min	Requirement
3	**Masses**								
3.1	Package mass			2,50		2,50	< 2,3	kg	Requirement
3.2	Battery mass total					3,00	1,70	kg	Request
3.2.1	Main Battery					2,00		kg	Request
3.2.2	Electronics Baterry					0,50		kg	Request
3.2.3	Extra battery for gliding under energy source fail					0,50		kg	Request
3.3	Wings					6,04		kg	Request
3.4	Skeleton (wingbox + Spars)					1,30		kg	Requirement
3.5	Fuselage (empty)					2,00		kg	Request
3.6	Loading mechanism					2,00		kg	Requirement
3.7	Stilts					1,20		kg	Request
3.8	Rotors, Motoren, Adapter, ESC Controller					4,50		kg	Requirement
3.9	Pylons and Nacelles					1,08		kg	Requirement
3.10	Hector Total Weight without package					18,12		kg	Requirement
3.11	Avionics					0,84		kg	Request
3.12	Camera		0,53		2,15	0,53		kg	Request
3.13	Cable		1,00		3,00	1,00		kg	Requirement
	Total mass					25,99	3,80	kg	Request
3.15	Moment of Inertia around Pitch Axis					919.107,84		kgmm^2	Request
4	**Material**								
4.1	Light weight					CFRP + Aluminium Mesh			Request
4.2	Stilts					Aluminium			Request
4.3	Inner spars					Polyurethane foam			Request
4.4	Loading mechanism	PBT = Polybutylenterephtalat				Iron + PBT plastic			Request
5	**Motion drive**								
5.1	Propulsion	High-Pole BLDC Motor				Electrical	Electrical		Request
5.2	Noise emissions		32 at cruise		50,00	84.84 (5m AGL)		dB	Request
6	**Power Source**								
6.1	Battery pack						LiPo 6S/10S 22,2/37 V		Request
6.1.1	Main Battery					14s3p			Request
6.1.2	Dedicated battery for the electronic					1s1p			Request
6.1.3	Security Battery for gliding					6s1p			Request
6.2	Capacity								
6.2.1	Lithium-metal					60.000,00		mAh	Request
6.2.2	Lithium-metal					2.000,00		mAh	Request
6.2.3	Hv LiPo					22.000,00	10.000,00	mAh	Request
7	**Avionics**								
7.1	Navigation systems	IMU e.g.: InvenSense MPU - 9250)				GNSS + IMU + Pseudolites + RAIM	Yes		Requirement
7.2	Digital pressure sensor + pitot tube					Yes			Request
7.3	Ultrasonic- & Infrared sensor					No			Request
7.4	Camera					Yes			Request
7.5	RADAR					Yes			Request
7.6	LiDAR sensor					No			Request
7.7	Miniaturized AoA/AoS sensors					Yes			Request
7.8	Gyroscope sensor					Yes, incl. in IMU			Requirement
7.9	Accelerometer					Yes, incl. in IMU			Requirement
7.10	Magnotemeter					Yes, incl. in IMU			Requirement
7.11	Barometer					Yes, incl. in IMU			Requirement
7.12	Detect And Avoid (DAA) system					RADAR + Camera + ADS-B Transponder	Sense and avoid		Requirement
7.13	Anti-Collision Lighting					Yes			Request
7.14	Identification system					Remote Identification + ADS-B Transponder			Requirement
8	**Security system**								
8.1	Software: Fail-Operate					Yes			Request
8.2	Hardware: Fail-Safe					Yes			Request
8.3	Anti-Spoofing					RAIM + Hybrid Algorithm			Request
8.4	Anti-Jamming/DoS					Hybrid Algorithm			Request
8.5	Anti-Injection					End-to-End Encryption			Request
9	**Energy Consumption**								
9.1	Total Motion Drive Maximum Power Output					18,68	4,00	kW	Request
9.2	Avionics					24,87		W	Request
9.3	Camera		25,00		35,00	35,00		W	Request
9.4	Anti-Collision Lighting		1,00		2,00	1,50		W	Request
	Total Power max.					18.739,44		W	
9.5	Roll-E Battery		22,20 V			0,45		Wh	Request
10	**Costs**								
10.1	Motion drive (Motor, ESC,Prop+Prop adapt)					4.791,30		€	Request
10.2	Battery	approximated				1.100,00		€	Request
10.3	Avionics								
10.3.1	Shock mounts		5,00		30,00	30,00		€	Requirement
10.3.2	Autopilot					205,00		€	Requirement
10.3.3	GNSS module		10,00		40,00	35,00		€	Request
10.3.4	IMU based on MEMS (magnetometer, accelerometer, gyroscope)			120,00		120,00		€	Request
10.3.5	Digital pressure sensor + pitot tube		13,00		56,00	36,00		€	Request
10.3.6	Miniaturized AoA/AoS sensors		200,00		600,00	400,00		€	Request
10.3.7	ADS-B Transponder		1.500,00		5.000,00	1.500,00		€	Requirement
10.3.8	RADAR		100,00		1.600,00	600,00			Requirement
10.4	Camera		350,00		4.000,00	890,00		€	Request
10.5	Anti-Collision Lighting			45,00		45,00		€	Request
10.6	Cable	incl. fibre optic	50,00		200,00	125,00		€	Requirement
10.7	Aircraft structure							€	Requirement
10.8	Loading mechanism					720,00		€	Requirement
	Total costs HecTO-R					10.597,30		€	
10.9	Battery Roll-E					194,95		€	Request
10.10	Total costs Roll-E					800,00		€	Request

Table 2: Top Level Aircraft Requirements Document

B. Conceptual Design

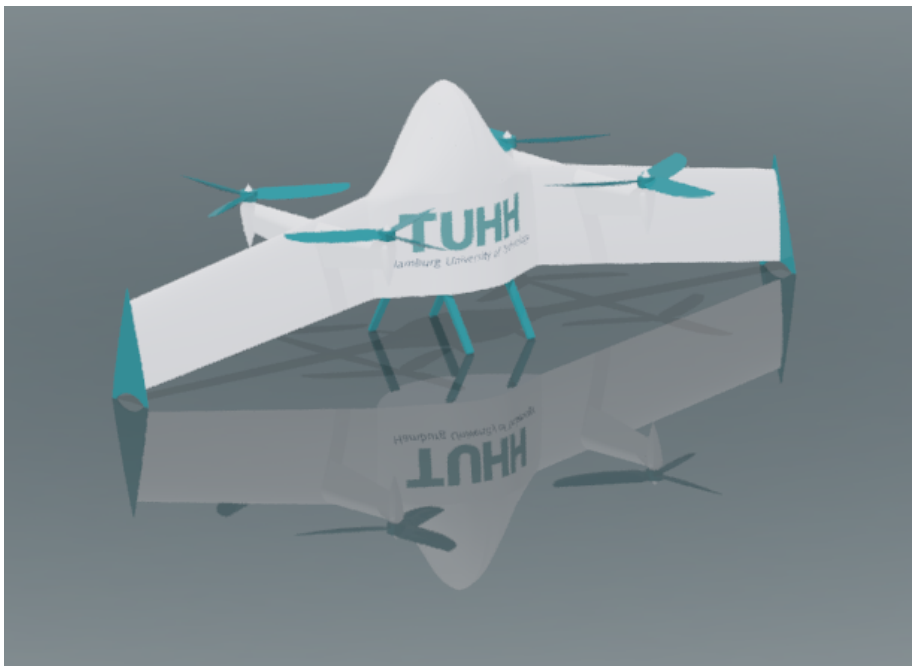

Figure 17: HecTO-R, CAD 3/4 view

C. Technical Design

C.1. Materials

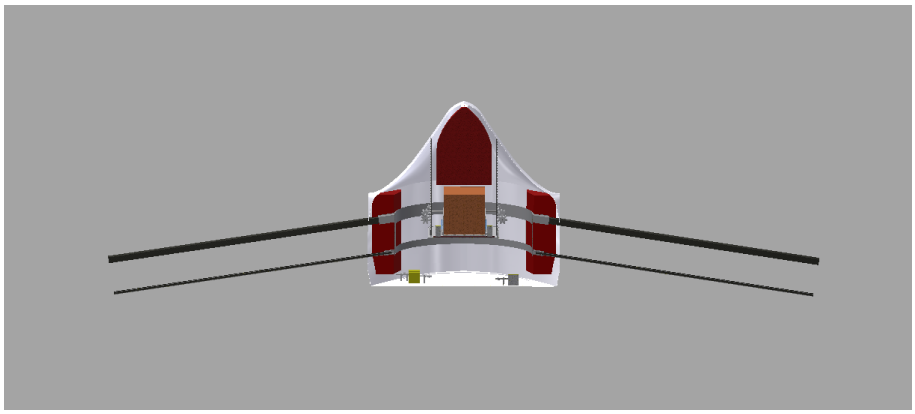

Figure 18: Structure incl. loading mechanism, main bay and side bays (both in red) for avionics and battery

C.2. Aerodynamics

C.2.1. Wing Values

Flying Wing Data		
Name	Value	Unit
Root Airfoil	MH-78	
Tip Airfoil	NACA 0012	
Reference Wing Area S	0,924	m^2
Wing Span b	2,75	m
Aspect Ratio	8,2	-
Root Length c_{root}	355,2	mm
Tip Length c_{tip}	316,67	mm
Taper Ratio λ	0,892	-
MAC Length $\bar{c}$	333,63	mm
X_{MAC} distance from reference	207,7	mm
Y_{MAC} distance from reference	674,4	mm
Quarter Chord Sweep Angle $\phi_{1/4}$	10	DEG
MAC incidence $i_{MAC}=a_{Cruise}$	4,52	DEG
Root incidence i_{Root}	5,5	DEG
Tip incidence i_{tip}	3,5	DEG

Table 3: Flying Wing Geometric Specifications

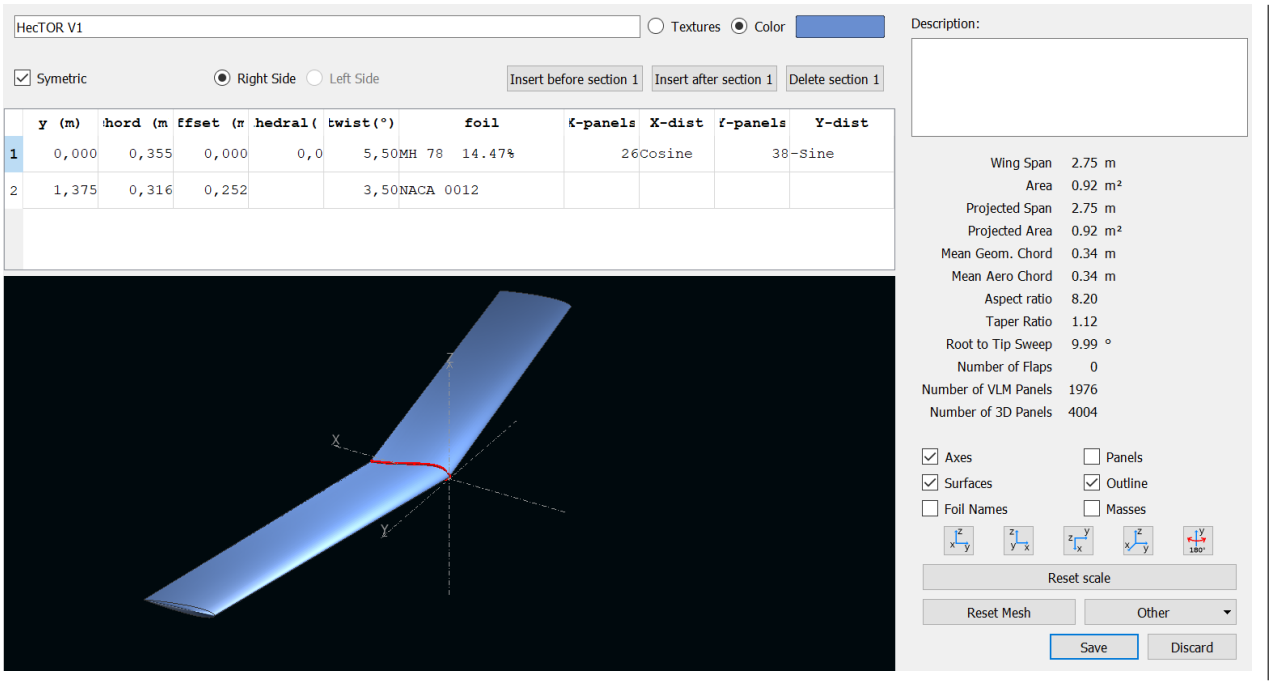

Figure 19: Analytically calculated input data for the flying wing simulation in XFLR5

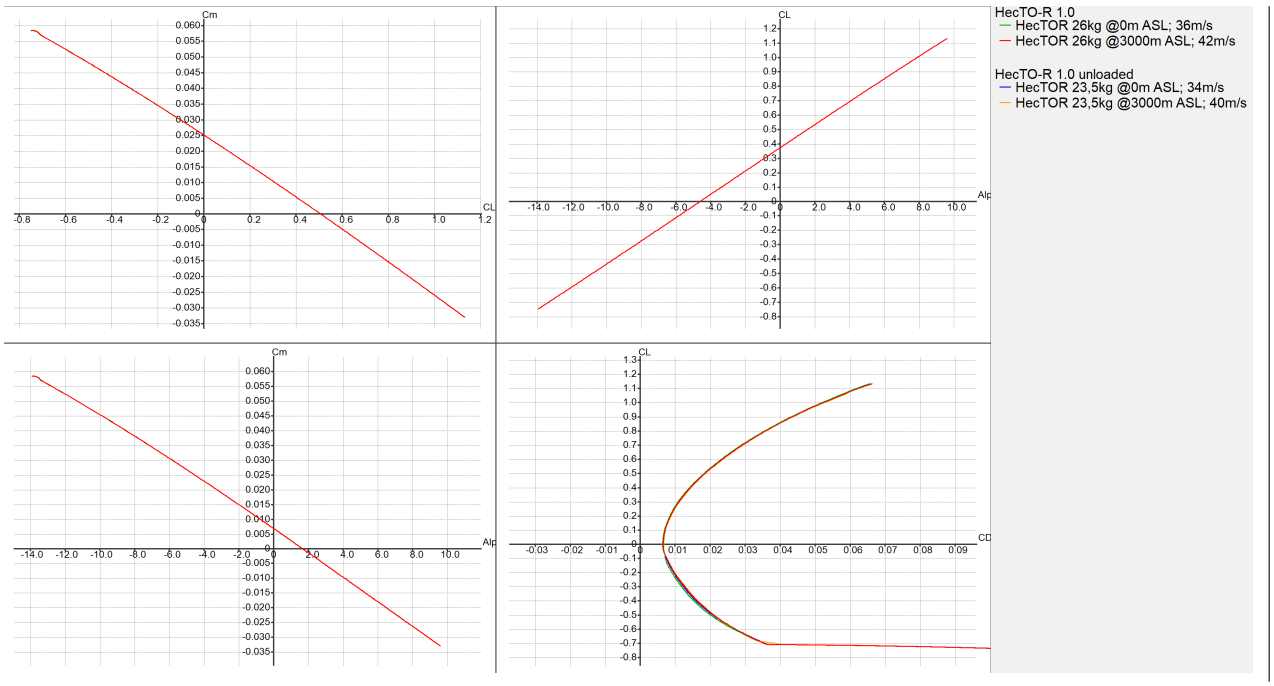

Figure 20: XFLR5 results of the flying wing for different flight configurations and conditions

C.3. Cargo

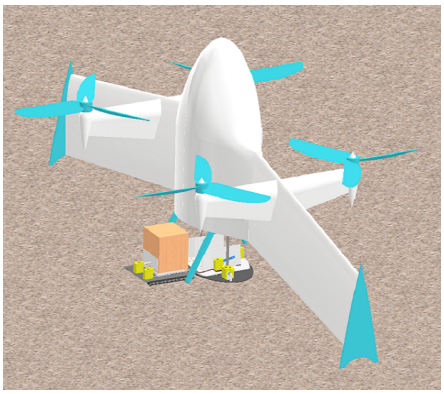

Figure 21: Loading mechanism, loading from Roll-E

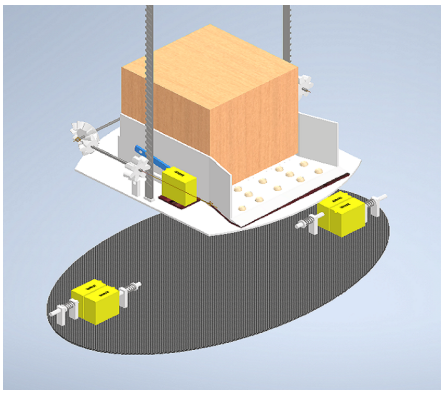

Figure 22: Loading mechanism, frontal view

C.4. Propulsion System

C.4.1. Motor

Motor Specifications		
Name	Value	Unit
Kv	120	RPM/V
Kt	0,0796	Nm/A
Km	0,1437	Nm/$\sqrt{W}$
Max continuous Current	110 (180s)	A
Max continuous Power	5695 (180s)	W
Voltage Range	22,2 – 60,9	V
Wind resistance	0,037	Ω
Stator poles	24	-
Magnetic poles	28	-
Motor Diameter	89	mm
Motor Length	49.2	mm
Motor Weight	760 (845 with wires)	g
Motor Timing	333,63	mm
ESC PWM Rate	207,7	mm

Table 4: Motor Specifications of a single motor

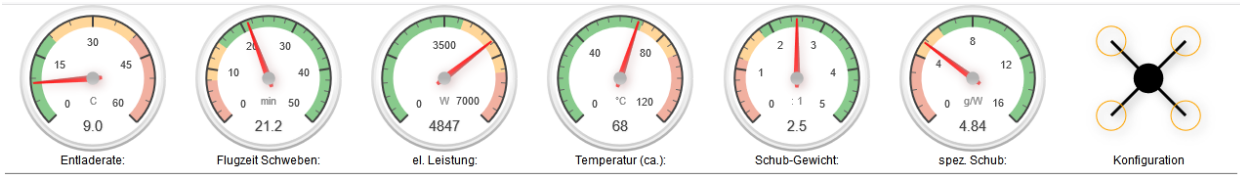

Anmerkungen:

Batterie		Motor @ Optimaler Wirkungsgrad		Motor @ Maximum		Motor @ Schweben		Gesamter Antrieb		Multikopter	
Entladerate:	9.00 C	Strom:	51.52 A	Strom:	90.04 A	Strom:	24.04 A	Komponenten:	9178 g	Abfluggewicht:	26000 g
Spannung:	54.67 V	Spannung:	55.05 V	Spannung:	53.83 V	Spannung:	55.93 V		323.7 oz		917.1 oz
Nennspannung:	53.48 V	Drehzahl*:	6358 U/min	Drehzahl*:	6025 U/min	Drehzahl*:	3510 U/min	Schub-Gewicht:	2.5 : 1	max. Zuladung:	29225 g
Energie:	2139.2 Wh	el. Leistung:	2836.5 W	el. Leistung:	4846.9 W	Regleröffnung (log):	38 %	Strom @ Schweben:	96.15 A		1030.9 oz
Gesamtkapazität:	40000 mAh	mech. Leistung:	2631.4 W	mech. Leistung:	4434.0 W	Regleröffnung (linear):	55 %	P(in) @ Schweben:	5450.7 W	max Neigung:	62 °
genutzte Kapazität:	34000 mAh	Wirkungsgrad:	92.8 %	Leistungs-Gewicht:	745.7 W/kg	el. Leistung:	1344.3 W	P(out) @ Schweben:	4951.2 W	max. Geschwindigkeit:	98 km/h
Flugzeit Vollgas:	5.7 min				338.2 W/lb	mech. Leistung:	1237.8 W	Wirkungsgrad @ Schweben:	90.8 %		60.9 mph
Ø Flugzeit:	18.1 min			Wirkungsgrad:	91.5 %	Leistungs-Gewicht:	209.6 W/kg	Strom @ max:	360.17 A	gesch. Reichweite:	7015 m
Flugzeit Schweben:	21.2 min			Temperatur (ca.):	68 °C		95.1 W/lb	P(in) @ max:	20417.4 W		4.36 mi
Gewicht:	4424 g				154 °F	Wirkungsgrad:	92.1 %	P(out) @ max:	17735.9 W	gesch. Steigleistung:	10.6 m/s
	156 oz					Temperatur (ca.):	36 °C	Wirkungsgrad @ max:	86.9 %		2087 ft/min

Table 5: Approximated Motor Performance

C.4.2. Electronic Speed Controller (ESC)

ESC Specifications		
Name	Value	Unit
Refresh Rate	2000 (50 – 2000)	Hz
Max Peak Current	220 (5s)	A
Max Peak Power	11395 (5s)	W
Max Continuous Current	125 (180s)	A
Max Continuous Power	6475 (180s)	W
Maximum efficiency	>98	%
Max RPM	360000	Ω
Weight	172 (220 with wires)	g

Table 6: Electronic Speed Controller Specifications

C.4.3. Battery

Battery Specifications		
Name	Value	Unit
Dimensions	80x91x10	mm
Material	Li-Metal	
Weight	0,158	g
Typical charge Current	10 (C/2)	A
Max continuous discharge	40 (2C)	A
Nominal voltage	3,82	V
Pulse discharge rate	100 (5C)	A
Capacity	20	Ah

Table 7: Battery Specifications

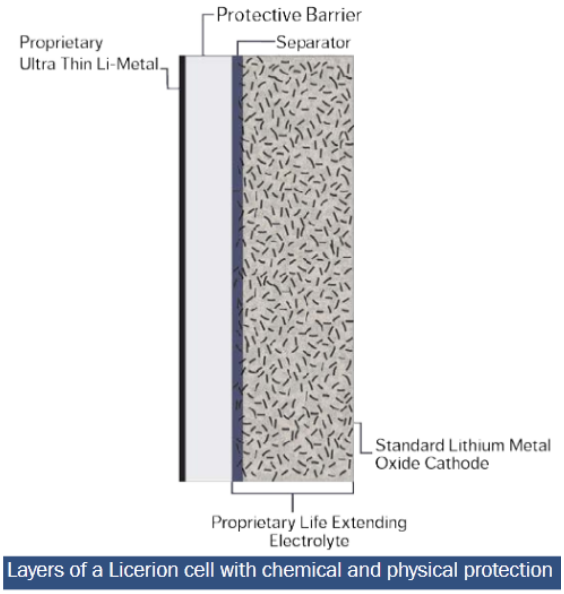

Figure 23: Metal technology from [Pow20a]

C.5. Avionics

C.5.1. Identification Systems

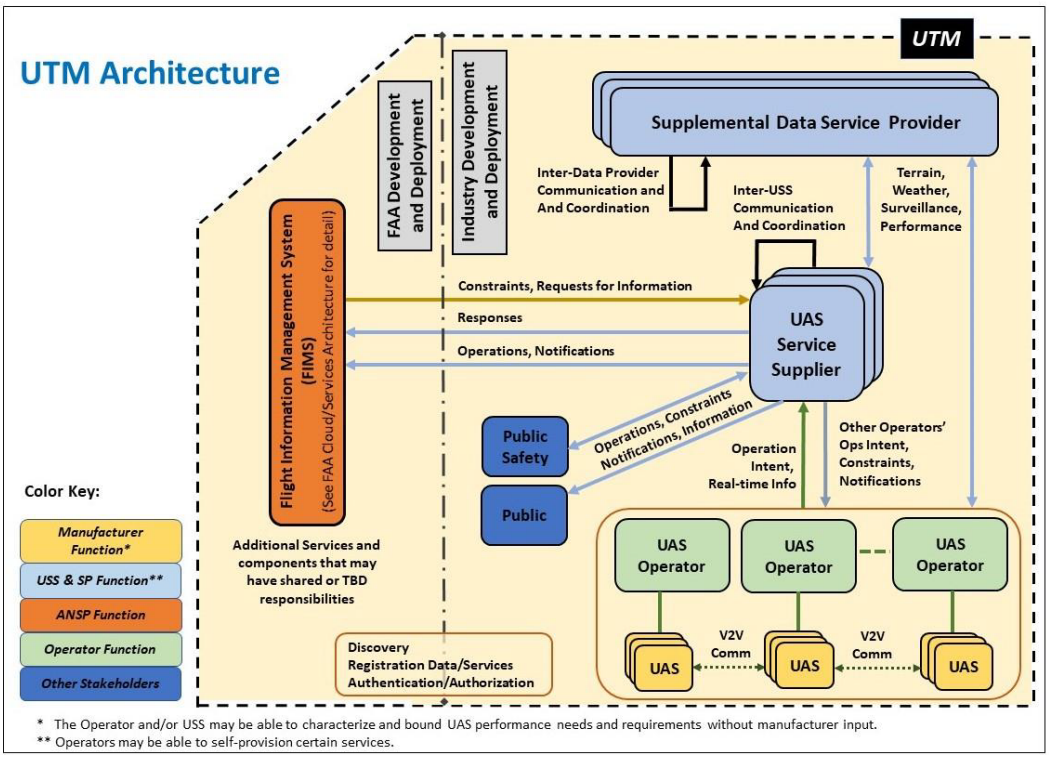

Figure 24: UTM architecture

C.5.2. Detect-and-avoid Systems

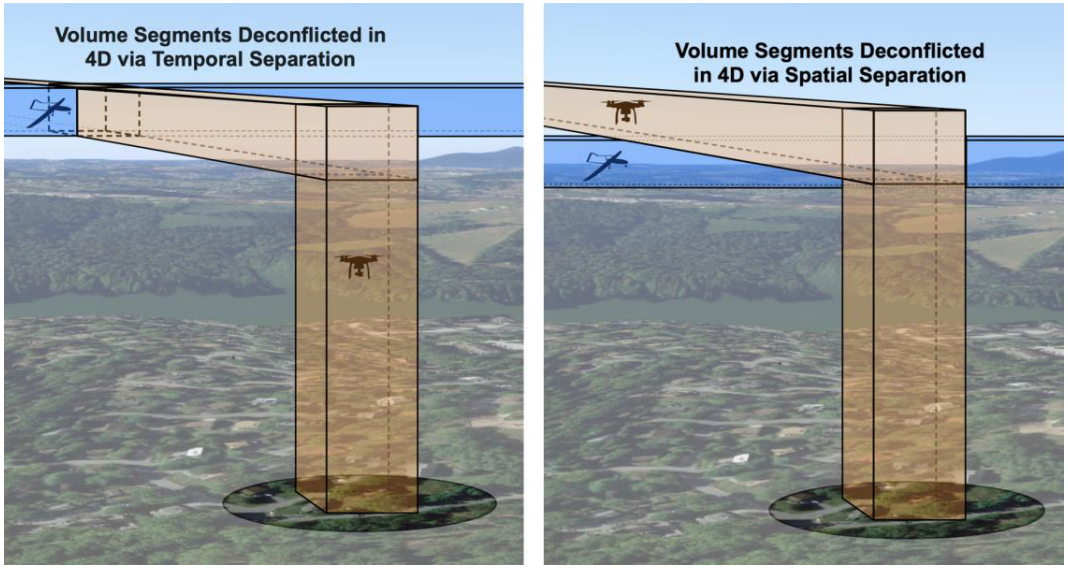

Figure 25: 4D trajectory separation from [al20]

Listing 1: Conceptual algorithm for visual detect and avoid system via trajectory adaptation based on [Sad20]

```
clc
clear all
Vbird=60*0.514; % velocity of bird [m/s]
Vhector=100*0.514; % velocity of HecTO-R [m/s]
psi_bird=65/57.3; % angle between horizontal axis and bird
psi_hector=140/57.3; %angle between horizontal axis and HecTO-R
Range=500; % Range of object detection by camera
dt = 0.01; % time interval in [sec]
xbird(1)=0; %initial bird position in x direction in [m]
ybird(1)=0; %initial bird position in y direction in [m]
xhector(1)=0; %initial HecTO-R position in x direction in [m]
yhector(1)=0; %initial HecTO-R position in y direction in [m]
for i = 1:1:1000
xbird(i+1)=Vbird*cos(psi_bird)*dt+xbird(i); %Trajectory calculated (wind
    effects incl.) and/or got from UTM network
xhector(i+1)=Vhector*cos(psi_hector)*dt+xhector(i);
ybird(i+1)=Vbird*sin(psi_bird)*dt+ybird(i); %Trajectory approximation by
    camera and/or RADAR
yhector(i+1)=Vhector*sin(psi_hector)*dt+yhector(i);
end
plot(xbird,ybird,'rO-',Range+xhector,yhector,'b*-'); grid
xlabel('X [m]')
ylabel('Y [m]')
legend('Bird','HecTO-R')
```

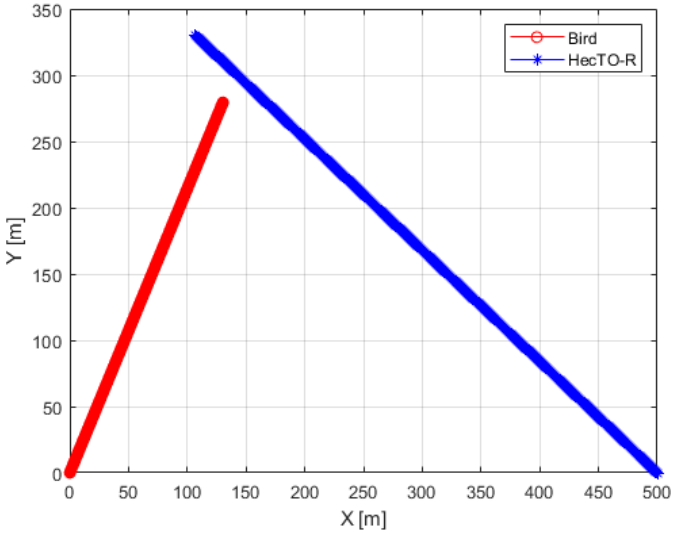

Figure 26: Avoidance concept via trajectory adaptation

D. Flight Performance

Aircraft Specifications		
Name	Value	Unit
Gross Weight	26	kg
Empty Weight (unloaded)	23,5	kg
Cruise Speed(s)	35 - 43	m/s
Stall Speed(s)	18,5 - 22,5	m/s
Negative Stall Speed(s)	23,5 - 29	m/s
Maximum Propeller Power (Total)	20	kW
Cruise Propeller Power (Total)	500-700	W
Lift-to-Drag Ratio @Cruise	23,3	-
Aircraft Range (Fully Charged)	> 60	km
Mission Duration (One-Way 15 km)	9 - 11	min
Maximum Wind Speeds @Cruise	11	m/s
Battery Weight (Total)	3	kg

Table 8: Flying Wing Performance Specifications

D.1. Flight Phase Performance

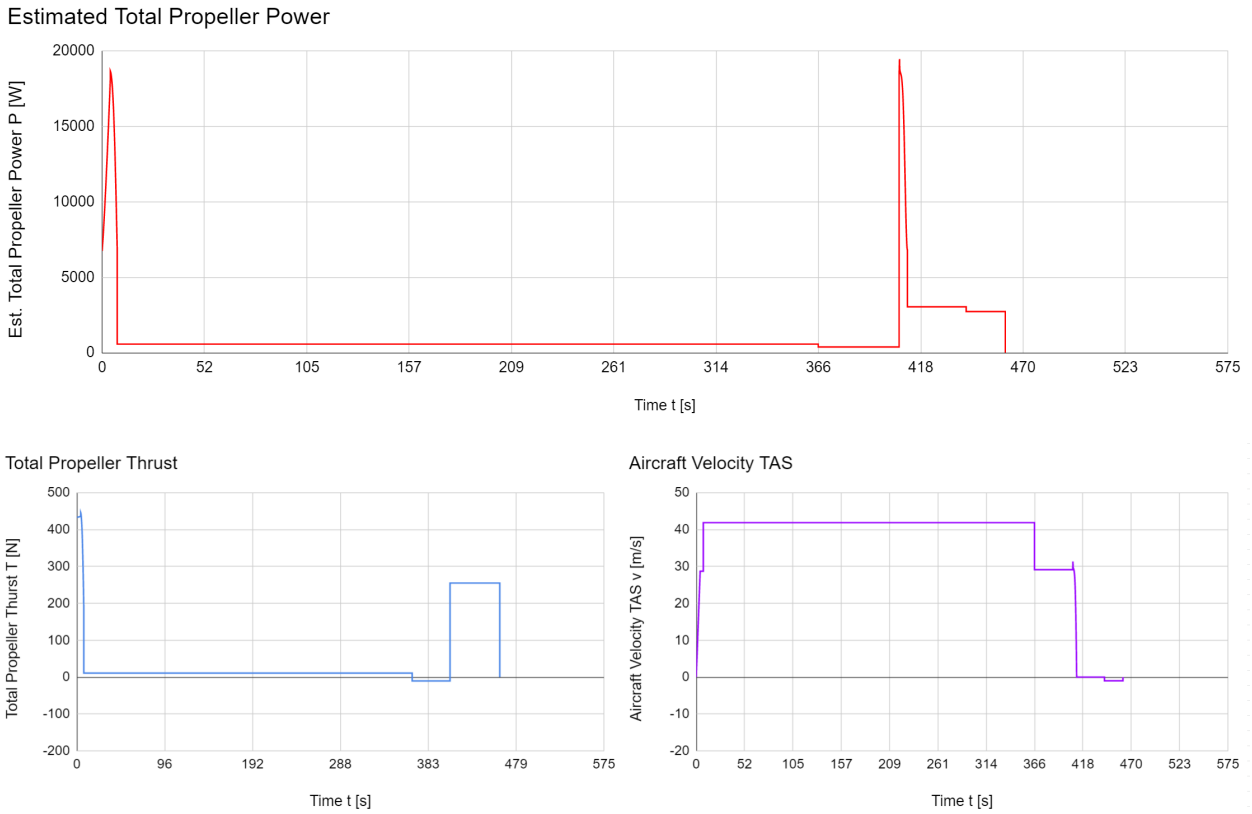

Figure 27: Flight performance curve of one loaded flight (26 kg) @3000m ASL

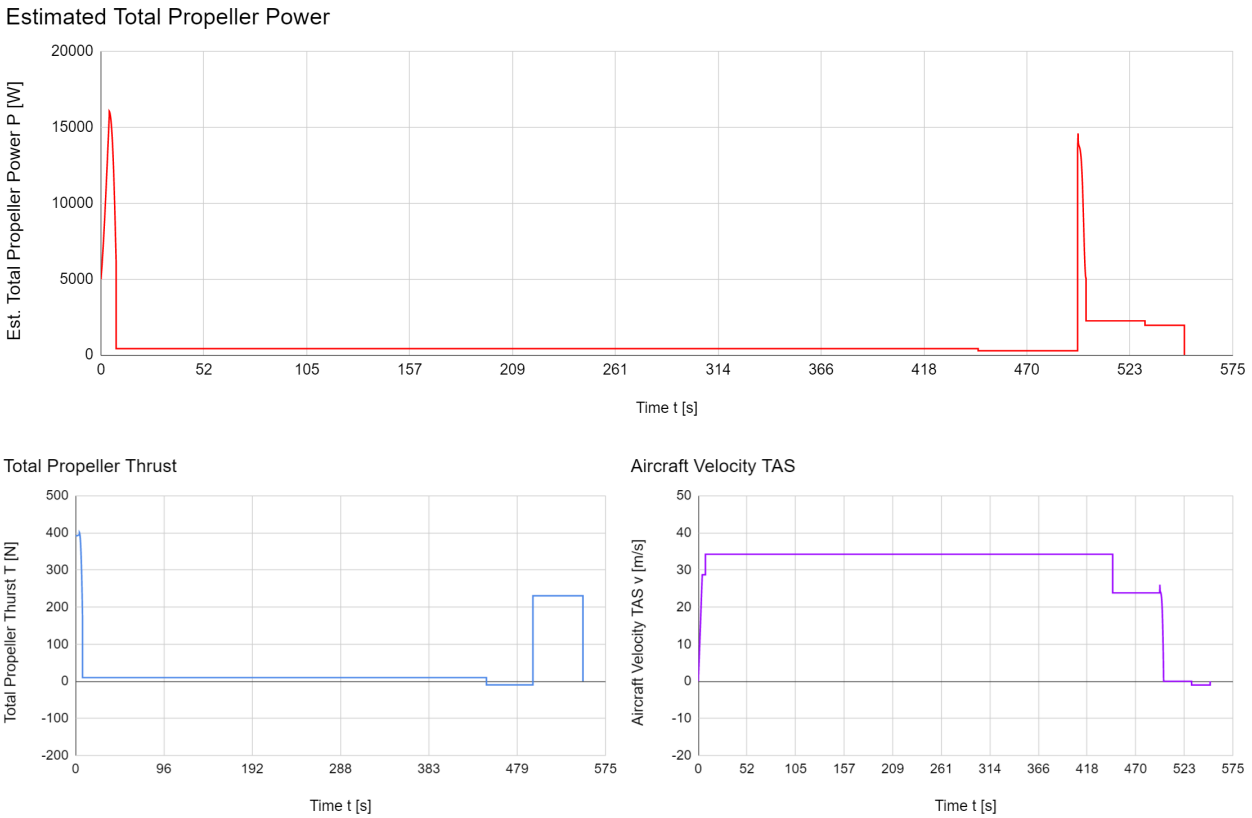

Figure 28: Flight performance curve of one unloaded flight (23.5 kg) @0m ASL

E. Operations & Costs

E.1. Non-Recurring Costs

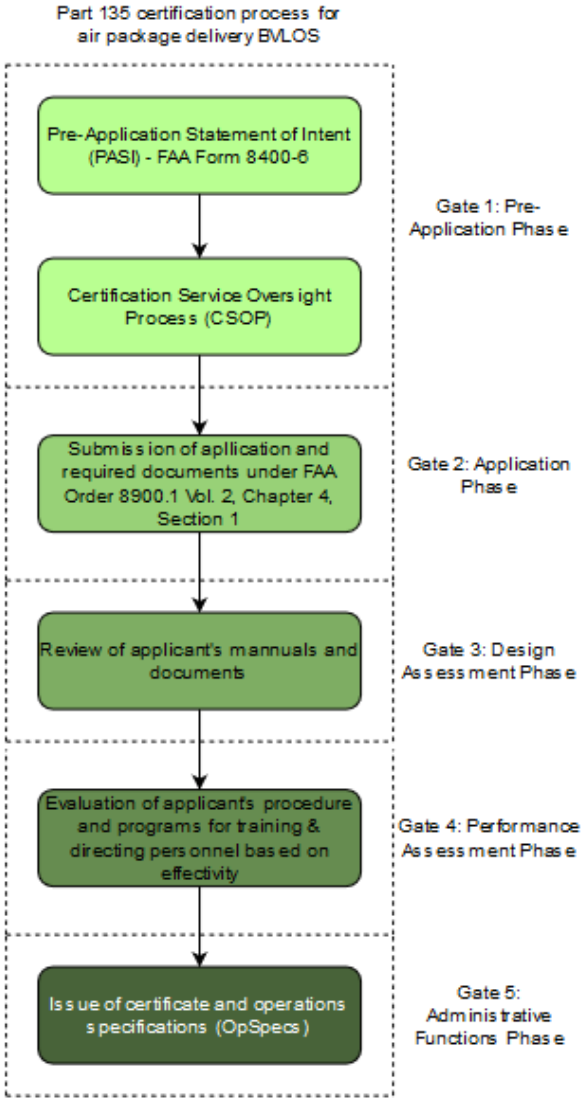

Figure 29: FAA Part 135 certification process

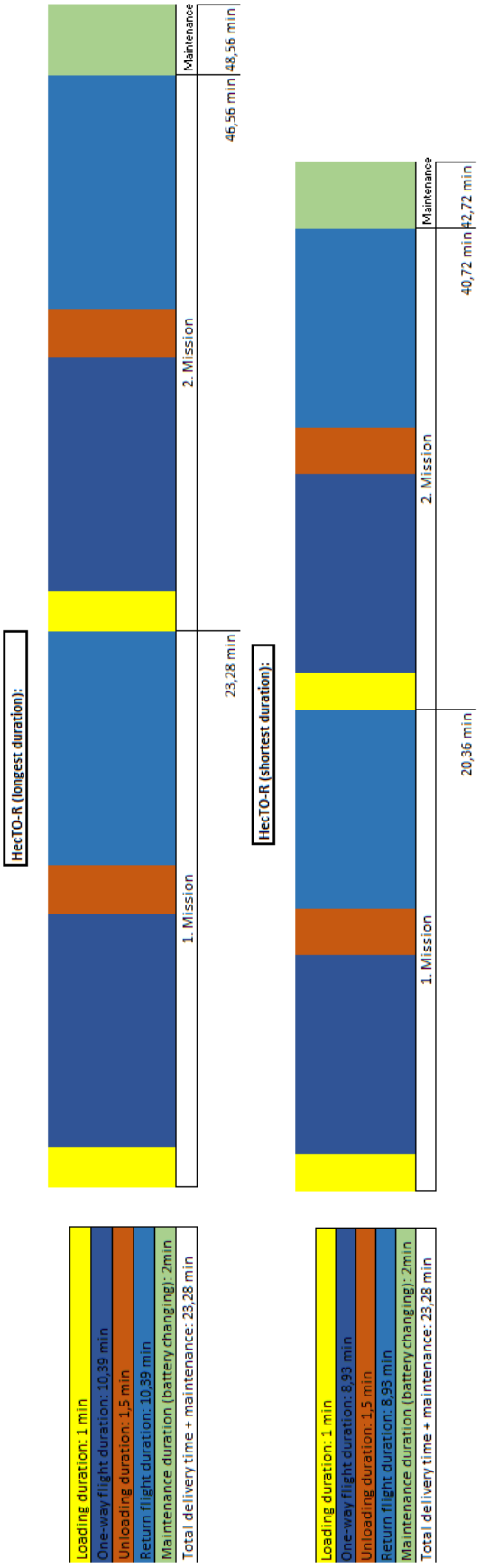

Figure 30: HecTO-R mission plan

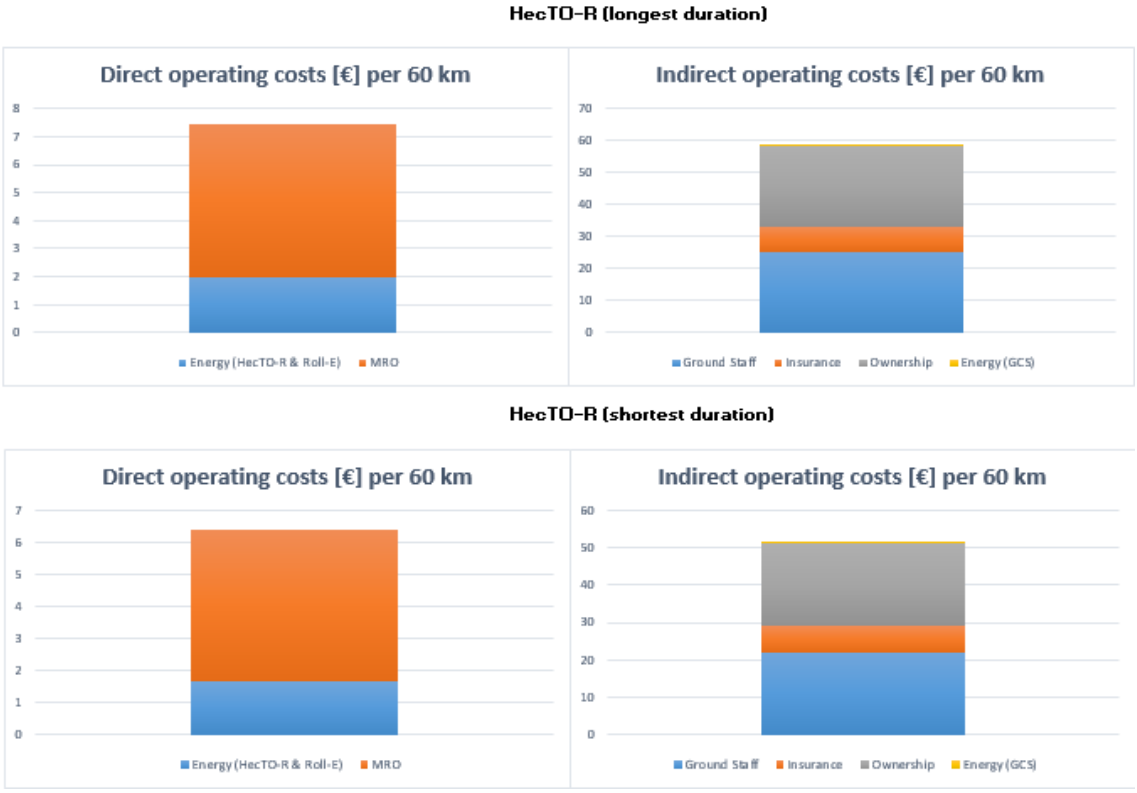

Figure 31: (In-)Direct operating costs for HecTO-R